Wefer, G., Berger, W.H., and Richter, C. (Eds.)
Proceedings of the Ocean Drilling Program, Scientific Results Volume 175

13. Data Report: Magnetic Properties and XRF-Scanner Data of Site 1075 (Lower Congo Basin)[1]

Carl Richter,[2] Peter Blum,[2] and Ursula Röhl[3]

ABSTRACT

We present sediment magnetic and chemical analysis of cyclic ocean sediments of the upwelling region of the Lower Congo Basin (equatorial Atlantic). We investigated two >100-k.y. intervals from Ocean Drilling Program Site 1075 to analyze the hysteresis properties, sources of magnetic susceptibility, anhysteretic remanent magnetizations, thermomagnetic behavior, and element concentrations of Fe, Ca, Ti, Mn, and K using an X-ray fluorescence (XRF) core scanner. The upper interval was sampled between 14 and 32 meters composite depth (mcd; 0.09–0.21 Ma) and the lower between 141 and 163 mcd (1.31–1.54 Ma) at a resolution of 20 cm, which represents a temporal resolution of 2.0 and 1.3 k.y., respectively. XRF core-scanner data were acquired at 5-cm intervals. The measurements show that ferri(o)magnetic minerals have no significant influence on the cyclicity of the magnetic susceptibility, which is dominated by paramagnetic and diamagnetic minerals and reflects changes of sediment input from the Congo River. The Fe, Ti, K, and Mn concentrations covary with the magnetic susceptibility where high concentrations of these elements correlate with intervals of high susceptibility and low concentrations with intervals of low susceptibility. The Ca counts correlate well with the calcium carbonate concentration but do not show the same cyclicity as the other elements or the susceptibility. With the exception of the Ca concentration, which is significantly higher in the upper interval, and the magnetic grain size, which indicates that less fine grained magnetite is present in the lower interval, no significant differences in the properties of the upper and the lower intervals were detected.

[1]Richter, C., Blum, P., and Röhl, U., 2001. Data report: Magnetic properties and XRF-scanner data of Site 1075 (Lower Congo Basin). *In* Wefer, G., Berger, W.H., and Richter, C. (Eds.), *Proc. ODP, Sci. Results,* 175, 1–31 [Online]. Available from World Wide Web: <http://www-odp.tamu.edu/publications/175_SR/VOLUME/CHAPTERS/SR175_13.PDF> [Cited YYYY-MM-DD]
[2]Ocean Drilling Program, Texas A&M University, College Station TX 77845-9547, USA. Correspondence author: richter@odpemail.tamu.edu
[3]Fachbereich Geowissenschaften, Universitt Bremen, D-28334 Bremen, Federal Republic of Germany.

Initial receipt: 4 September 2000
Acceptance: 23 October 2000
Web publication: 4 June 2001
Ms 175SR-214

INTRODUCTION

The Congo River Basin is one of the largest drainage basins in the world. The materials deposited by its main rivers provide the opportunity to study the products of denudation of a large fraction of the upper continental crust of the African continent (Fig. F1). This report characterizes different phases carried by the Congo rivers and deposited into the Lower Congo Basin by using magnetic properties and high-resolution X-ray fluorescence (XRF) core-scanner measurements as proxies for the changing sediment input. The depositional system at Site 1075 in the Lower Congo Basin includes the sediment-producing drainage basin of the Congo River with processes that include river transport, redistribution (including possible intermediate storage on the shelf), and marine processes (Jansen et al., 1984; Olausson, 1984; Jansen and van Iperen, 1991; Wefer et al., 1996; Schneider et al., 1994, 1996, 1997; Berger et al., 1998a, 1998b). Marine factors include primarily productivity patterns of both the open ocean and the coastal ocean as well as the changing carbonate chemistry of deep waters. The production of sediment in the Congo Basin is largely a function of the wetness of the climate on the African continent (Jansen, 1990). Ocean productivity is a function of winds, which in the tropical Atlantic depend on monsoonal amplitudes and the nutrient supply within the thermocline waters.

Site 1075 was drilled during Ocean Drilling Program (ODP) Leg 175 (Wefer, Berger, Richter, et al., 1998) in the equatorial Atlantic Ocean (4°47.12′S, 10°4.50′E). The site is located in 2995-m-deep water in an environment dominated by sediment input from the Congo River, seasonal coastal upwelling and associated filaments and eddies moving offshore, and incursions of open-ocean waters from the South Equatorial Countercurrent.

Three holes were cored with the advanced hydraulic piston corer to a maximum depth of 207.2 meters below seafloor (mbsf), which recovered a continuous Pleistocene to late Pliocene-age interval (Wefer, Berger, Richter, et al., 1998). A spliced record using sediment cores from all three holes was constructed and yielded a complete stratigraphic sequence with no significant coring gaps. The recovered materials are cyclic deep-sea sediments, which consist of greenish gray diatomaceous clay and nannofossil-bearing diatomaceous clay. Sedimentation rates for the recovered sequence are high and average 100 m/m.y., which permits the determination of records with excellent temporal resolution.

High-resolution shipboard measurements of physical properties such as magnetic susceptibility (Fig. F2), color reflectance, and gamma-ray attenuation from Site 1075 material vary on orbital time scales and show an excellent correlation to the global oxygen isotope curve (Berger et al., 1998a). Magnetic susceptibility has been frequently compared to commonly known paleoclimate indicators such as calcium carbonate percentages and oxygen isotopes in deep-sea sediments (e.g., Bloemendal et al., 1988; Bloemendal and deMenocal, 1989; Kukla et al., 1988).

We performed detailed rock magnetic measurements on 218 discrete samples from the composite section of two depth intervals at Site 1075 (Fig. F2). The younger interval was sampled between 14 and 32 meters composite depth (mcd) (0.09–0.21 Ma) and the older between 141 and 163 mcd (1.31–1.54 Ma) at a resolution of 20 cm, which represents a temporal resolution of 2.0 and 1.3 ka, respectively. These intervals were

F1. Location map of Site 1075 in the Lower Congo Basin, p. 9.

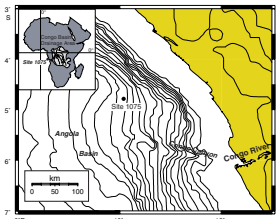

F2. Susceptibility record of the composite section at Site 1075, p. 10.

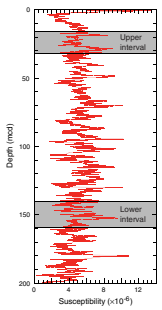

also measured with an XRF core scanner (Jansen et al., 1998) at 5-cm resolution to obtain the geochemical composition of the sediment.

SAMPLING AND EXPERIMENTAL PROCEDURES

Volume-normalized magnetic susceptibility (*k*) on the *JOIDES Resolution* was measured at a spacing of 2 cm on Site 1075 whole-core sections using a Bartington Instruments MS-2 susceptibility meter. The sensing loop has an 80-mm diameter and uses an inducing field of 0.1 mT at a frequency of 565 Hz. The meter was set on SI units and the raw values were converted to SI volume-normalized susceptibilities.

We took 218 samples (wet volume = ~7 cm^3) for detailed rock magnetic characterization from two depth intervals at Cores 175-1075-3H through 5H, between 14 and 32 mcd (0.21–0.09 Ma), and the older at Cores 175-1075A-15H through 16H, between 141 and 163 mcd (1.31–1.54 Ma). Sampling was conducted at one sample every 20 cm, or at ~1.3 and 2.0 k.y., respectively (Table T1). The comparison between samples from different holes is possible by using the meters composite depth scale, which was established by interhole correlation procedures during Leg 175 (Berger et al., 1998a; see also Hagelberg et al., 1992, for procedures). Samples from the Hole 1075B part of the splice are included in Table T1 but are not represented in the figures because of a mismatch in the composite depth section.

T1. Rock-magnetic data, Site 1075, p. 16.

The low-field mass-normalized susceptibility (*c*) of the specimens was measured using a KLY-2 Kappabridge (Geofyzika Brno; inducing field = 0.5 mT) at the Institute for Rock Magnetism at the University of Minnesota. Hysteresis properties were determined on the Princeton Measurements Corporation vibrating sample magnetometer (microVSM) at the Institute for Rock Magnetism. An anhysteretic remanent magnetization (ARM) was imparted to each sample by exposing it to a constant 0.05-mT field and a slowly decaying 100-mT field. Partial anhysteretic remanence magnetizations (pARM) were imparted on 13 selected samples by switching on a direct current field between two specified values of alternating field. Grains with coercivity within that window acquire an ARM while the rest of the assemblage is demagnetized. By moving the window over a range of alternating fields, a pARM curve is obtained, representing the spectrum of coercivities in the sample (Jackson et al., 1988; Jackson et al., 1989). A 1-T isothermal remanent magnetization (IRM) was imparted with an ASC IM-10 impulse magnetizer and a backfield isothermal remanent magnetization (BIRM) imparted at –0.3 T. The acquired magnetizations were measured using the 2G three-axis superconducting rock magnetometer at the Institute for Rock Magnetism. Low-temperature demagnetization of the saturation isothermal remanent magnetization was conducted on a Quantum Design magnetic property measuring system. A 2.5-T field was imparted at 20 K and the magnetic moment was recorded in 5-K steps during the warm up from 20 to 300 K in zero field.

We used the XRF core scanner (Jansen et al., 1998; Röhl and Abrams, 2000) at the University of Bremen to determine the chemical element composition of the two depth intervals. The XRF core scanner is a nondestructive analysis system developed to scan the surface of split cores at high resolution. The central sensor unit consists of a molybdenum X-ray source (3–50 kV) and a Peltier-cooled Si (PSI) detector (KEVEX) with a 125-µm beryllium window and a multichannel analyzer with a 20-eV spectral resolution. The system is computer controlled and allows the

analysis of elements from the atomic number 19 through 38 (K through Sr). The analyses were performed at predetermined positions and counting times. The X-ray source and the detector are lowered on the core surface during analysis; a slit defines the dimensions of the irradiated 1-cm² core surface. The analyzed area is flushed with helium gas to avoid a loss of energy because of scattering in air. The XRF data of all split sections were collected at 5-cm intervals over a 1-cm² area. A test-run calibration resulted in the use of a 15-s count time and an X-ray current of 0.15 mA to obtain statistically significant data of the investigated elements (K, Ca, Fe, Ti, and Mn). Although Sr and Cu measurements were also obtained, the counts at the selected counting time were too low to be interpreted.

RESULTS

Thermomagnetic Behavior, Hysteresis Properties, and pARM

The low-temperature experiments (Fig. **F3**) show a rapid loss of magnetization between 10 (20) and 50 K, which is caused by the transition from ferromagnetic to paramagnetic properties of the clay minerals. Samples from the lower interval were cooled to 10 K and show an intensity loss of as much as 65% by the time they have been heated to 20 K. None of the investigated samples shows any of the typical and well-known phase transitions of ferri(o)magnetic minerals.

Hysteresis measurements were only performed on a subset of 20 samples, because the remanent properties of the material were too weak even after significant averaging times (up to 10 s per measurement point on the VSM) to produce measurements of the entire sample set. Eleven of the samples contained sufficient magnetic material to yield hysteresis parameters (Table **T2**). Figure **F4** shows examples of hysteresis loops with a small but detectable ferrimagnetic contribution. Correction for the high-field slope of the loop (Fig. **F4B, F4D**) yields ferrimagnetic hysteresis curves with parameters that are likely to be magnetite. The coercivity H_c ranges from 3.98 to 10.4 mT (8.1 mT average) and the saturation remanence (M_r) to saturation magnetization (M_s) ratio from 0.042 to 0.144 (0.098 average), which suggests that pseudo-single-domain (PSD)-sized magnetite is probably the dominant magnetic carrier mineral.

The hysteresis loops show also that a significant difference between the high-field and the low-field susceptibility does not exist, which demonstrates that the low-field susceptibility is dominated by the paramagnetic (clay) minerals.

Under the assumption that magnetite is the only mineral contributing to room temperature hysteresis, the amount of magnetite can be calculated from the saturation magnetization M_s extrapolated to zero field. The percentage of magnetite is the M_s of the sample divided by the M_s of pure magnetite (92 Am²/kg) multiplied by 100. The magnetite concentration determined by this method is very low and varies from 5.28 to 5.53 ppm (average = 1.42 ppm) (Table **T2**).

Acquisition of pARMs was performed on 13 samples (Fig. **F5**). The shape of the curves in the upper interval (Fig. **F5A**) varies considerably, but the maximum pARM that can be imparted is centered between 10 and 20 mT (arrow in Fig. **F5**). This is typical for PSD magnetite with a

F3. Low-temperature demagnetizations of IRM, p. 11.

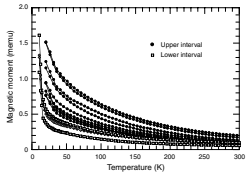

T2. Hysteresis properties and estimated magnetic concentrations, p. 20.

F4. Hysteresis measurements before and after high-field slope correction, p. 12.

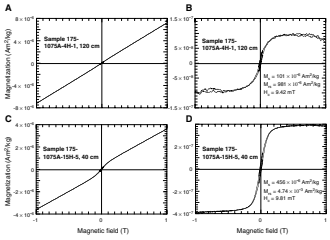

F5. Partial ARM acquisition curves, p. 13.

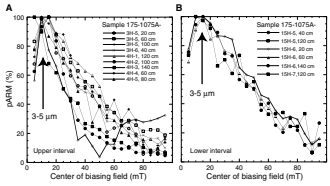

grain size between 3 and 5 µm (Jackson et al., 1988, 1989). Shallow slopes at higher alternating fields represent sediments with a broader range of coercivities and, hence, grain sizes than steeper curves. A difference between samples from low-susceptibility and high-susceptibility intervals does not exist. Samples from the lower interval (Fig. F5B) display a consistently broader distribution of magnetic grain sizes indicated by the shallow slope of the curves. As in the upper interval, the maximum pARM that can be imparted is between 10 and 20 mT, indicating a magnetic grain size between 3 and 5 µm.

Magnetic Susceptibility, ARM, and IRM

Figure F6 shows the shipboard volume susceptibilities for the upper and lower interval in addition to the mass susceptibility, ARM, IRM, S-ratio (= IRM – 0.3 T/IRM 1T), and k_{ARM}/χ as a function of depth. The mass susceptibilities are low and range from 5.80×10^{-8} to 1.52×10^{-7} m^3/kg. The mean value for the upper interval is 1.08×10^{-7} m^3/kg and is slightly lower with 8.45×10^{-8} m^3/kg in the lower interval.

The ARM is 3.70 µAm²/kg in the upper interval and 2.79 µAm²/kg in the lower interval on average. The average IRM at 1 T is 191.1 µAm²/kg in the upper interval and 184.9 µAm²/kg in the lower interval. The remanent magnetizations show variations that are apparently not correlated to the magnetic susceptibility (Fig. F6). Shaded bars in Figure F6 highlight horizons with high magnetic susceptibility values for comparison. The S-ratio stays relatively constant at 0.89 (0.88) in the upper (lower) interval. The S-ratio indicates the presence of a small high-coercivity phase, which is independent of the susceptibility variation.

The k_{ARM}/χ ratio is frequently used as a magnetic grain-size indicator (e.g., Thomson and Oldfield, 1986; Verosub and Roberts, 1995). In both depth intervals, the k_{ARM}/c ratio is negatively correlated with the magnetic susceptibility, which could be interpreted as an increase in magnetic grain size in intervals of high magnetic susceptibility (Fig. F6). We have demonstrated above that the susceptibility measures predominantly the paramagnetic (clay) fraction, whereas the ARM as a remanence measures the fine-grained ferrimagnetic (magnetite) fraction. Because the magnetic susceptibility and the ARM measure different minerals, the interpretation of the k_{ARM}/c ratio as a magnetic grain size indicator at Site 1075 is not straightforward. The ARM/IRM ratio is a ratio of two remanent magnetizations and thus is not influenced by paramagnetic phases. It can be used as a magnetic grain-size indicator because the ARM is more effective in activating finer magnetite grains than the IRM. Figure F6 shows that the ratio is smaller on average in the lower interval (mean = 0.016) than in the upper interval (mean = 0.021), indicating that the lower interval contains less fine-grained magnetite than the upper interval. A relationship between the grain size indicator and high- or low-susceptibility horizons is not apparent.

XRF-Scanner Results

The XRF-scanner results for K, Ca, Ti, Mn, and Fe for the two depth intervals are displayed together with the magnetic susceptibility on the left panel for reference (Fig. F7; Table T3). The Fe counts are the highest and the Mn counts are the lowest and exhibit the largest scatter. All elemental counts, except for the Ca counts, correlate well with the magnetic susceptibility record. The Ca counts correlate well with the $CaCO_3$

F6. Rock-magnetic properties of two depth intervals, p. 14.

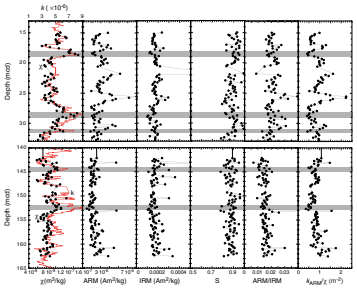

F7. XRF core-scanner data of the upper and lower intervals, p. 15.

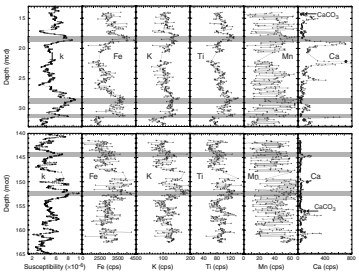

T3. XRF core-scanner results and interpolated shipboard susceptibility data, p. 21.

concentration (Fig. F7) but do not show the same cyclicity as the other elements or the magnetic susceptibility. Differences in element counts are <5% between the two intervals for K, Ti, and Fe and 14% for Mn. The Ca counts are significantly higher in the upper interval (average = 150 cps) than in the lower interval (average = 52 cps). The downhole decrease in carbonate concentration is also evident from the data published by Berger et al. (1998a). The $CaCO_3$ concentrations are only a few weight percent and too low to have a significant dilution effect on the magnetic susceptibility signal.

The magnetic susceptibility is an excellent proxy for element concentrations that are driven by climate cycles. The observed cycles reflect climate-driven changes in the sediment composition where warm climates are characterized by high susceptibilities (Berger et al., 1998; Dupont et al., submitted [N1]), and according to the presented data, higher Fe, Ti, Mn, and K concentrations. With the exception of the Ca concentration and the magnetic grain size, no significant differences in the properties of the upper and the lower interval were found.

ACKNOWLEDGMENTS

We thank members of the ODP Leg 175 shipboard scientific party, especially shipboard paleomagnetists Gina Frost, Toshi Yamazaki, and Peter Solheid, for numerous discussions and acknowledge the support and cooperation of the ODP personnel, Captain T. Ribbens, and the crew of the *JOIDES Resolution*. Thorough reviews by Stefanie Brachfeld and ODP Editor John Scroggs improved the manuscript. We thank the Institute for Rock Magnetism for the use of its facilities and its outstanding scientific and technical support. The Institute for Rock Magnetism is funded by the Keck Foundation, the National Science Foundation, and the University of Minnesota. This research was supported by U.S. Science Support Program JOI/USSSP grant 175-F000863 and the Deutsche Forschungsgemeinschaft.

REFERENCES

Berger, W.H., Wefer, G., Richter, C., Lange, C.B., Giraudeau, J., Hermelin, O., and Shipboard Scientific Party, 1998a. The Angola-Benguela upwelling system: paleoceanographic synthesis of shipboard results from Leg 175. *In* Wefer, G., Berger, W.H., and Richter, C., et al., *Proc. ODP, Init. Repts.,* 175: College Station, TX (Ocean Drilling Program), 505–531.

Berger, W.H., Wefer, G., Richter, C., and Shipboard Scientific Party, 1998b. Color cycles in Quaternary sediments from the Congo Fan region (Site 1075): a statistical analysis. *In* Wefer, G., Berger, W.H., and Richter, C., et al., *Proc. ODP, Init. Repts.,* 175: College Station, TX (Ocean Drilling Program), 561–567.

Bloemendal, J., and deMenocal, P., 1989. Evidence for a change in the periodicity of tropical climate cycles at 2.4 Myr from whole-core magnetic susceptibility measurements. *Nature,* 342:897–900.

Bloemendal, J., Lamb, B., and King, J., 1988. Paleoenvironmental implications of rock-magnetic properties of late Quaternary sediment cores from the eastern equatorial Atlantic. *Paleoceanography,* 3:61–87.

Hagelberg, T., Shackleton, N., Pisias, N., and Shipboard Scientific Party, 1992. Development of composite depth sections for Sites 844 through 854. *In* Mayer, L., Pisias, N., Janecek, T., et al., *Proc. ODP, Init. Repts.,* 138 (Pt. 1): College Station, TX (Ocean Drilling Program), 79–85.

Jackson, M., Gruber, W., Marvin, J., and Banerjee, S.K., 1988. Partial anhysteretic remanence and its anisotropy: applications and grainsize-dependence. *Geophys. Res. Lett.,* 15:440–443.

Jackson, M., Sprowl, D., and Elwood, B.B., 1989. Anisotropies of partial and anhysteretic remanence and susceptibility in compacted black shales: grainsize- and composition-dependent magnetic fabric. *Geophys. Res. Lett.,* 16:1063–1066.

Jansen, J.H.F., 1990. Glacial-interglacial oceanography of the southeastern Atlantic Ocean and the paleoclimate of west central Africa. *In* Lanfranchi, R., and Schwartz, D. (Eds.), *Paysages Quaternaires de l'Afrique Centrale Atlantique:* Paris (Editions ORSTOM), 110–123.

Jansen, J.H.F., Van der Gaast, S.J., Koster, B., and Vaars, A.J., 1998. CORTEX, a shipboard XRF-scanner for element analyses in split sediment cores. *Mar. Geol.,* 151:143–153.

Jansen, J.H.F., and van Iperen, J.M., 1991. A 220,000-year climatic record for the east equatorial Atlantic Ocean and equatorial Africa: evidence from diatoms and opal phytoliths in the Zaire (Congo) deep-sea fan. *Paleoceanography,* 6:573–591.

Jansen, J.H.F., van Weering, T.C.E., Gieles, R., and van Iperen, J., 1984. Middle and late Quaternary oceanography and climatology of the Zaire-Congo fan and the adjacent eastern Angola Basin. *Neth. J. Sea Res.,* 17:201–249.

Kukla, G., Heller, F., Ming, L.X., Chun, X.T., Sheng, L.T., and Sheng, A.Z., 1988. Pleistocene climates in China dated by magnetic susceptibility. *Geology,* 16:811–814.

Olausson, E., 1984. Oxygen and carbon isotope analyses of a Late Quaternary core in the Zaire (Congo) fan. *Neth. J. Sea Res.,* 17:276–279.

Röhl, U., and Abrams, L.J., 2000. High-resolution, downhole, and nondestructive core measurements from Sites 999 and 1001 in the Carribean Sea: application to the late Paleocene Thermal Maximum. *In* Leckie, R.M., Sigurdsson, H., Acton, G.D., and Draper, G. (Eds.), *Proc. ODP, Sci. Results,* 165: College Station, TX (Ocean Drilling Program), 191–203.

Schneider, R., Müller, P.J., and Wefer, G., 1994. Late Quaternary productivity changes off the Congo deduced from stable carbon isotopes of planktonic foraminifera. *Palaeogeogr., Palaeoclimatol., Palaeoecol.,* 110:255–274.

Schneider, R.R., Müller, P.J., Ruhland, G., Meinecke, G., Schmidt, H., and Wefer, G., 1996. Late Quaternary surface temperatures and productivity in the east-equatorial South Atlantic: response to changes in trade/monsoon wind forcing and surface

water advection. *In* Wefer, G., Berger, W.H., Siedler, G., and Webb, D. (Eds.), *The South Atlantic: Present and Past Circulation:* Berlin (Springer-Verlag), 527–551.

Schneider, R.R., Price, B., Müller, P.J., Kroon, D., and Alexander, I., 1997. Monsoon-related variations in Zaire (Congo) sediment load and influence of fluvial silicate supply on marine productivity in the east equatorial Atlantic during the last 200,000 years. *Paleoceanography,* 12:463–481.

Thompson, R., and Oldfield, F., 1986. *Environmental Magnetism:* London (Allen and Unwin).

Verosub, K.L., and Roberts, A.P., 1995. Environmental magnetism: past, present, and future. *J. Geophys. Res.,* 100:2175–2192.

Wefer, G., Berger, W.H., Siedler, G., and Webb, D.J. (Eds.), 1996. *The South Atlantic: Present and Past Circulation:* Berlin (Springer-Verlag).

Wefer, G., Berger, W.H., and Richter, C., et al., 1998. *Proc. ODP, Init. Repts.,* 175: College Station, TX (Ocean Drilling Program).

Figure F1. Location map of Site 1075 in the Lower Congo Basin. Inset shows the Congo Basin drainage area and Site 1075 in reference to the African continent.

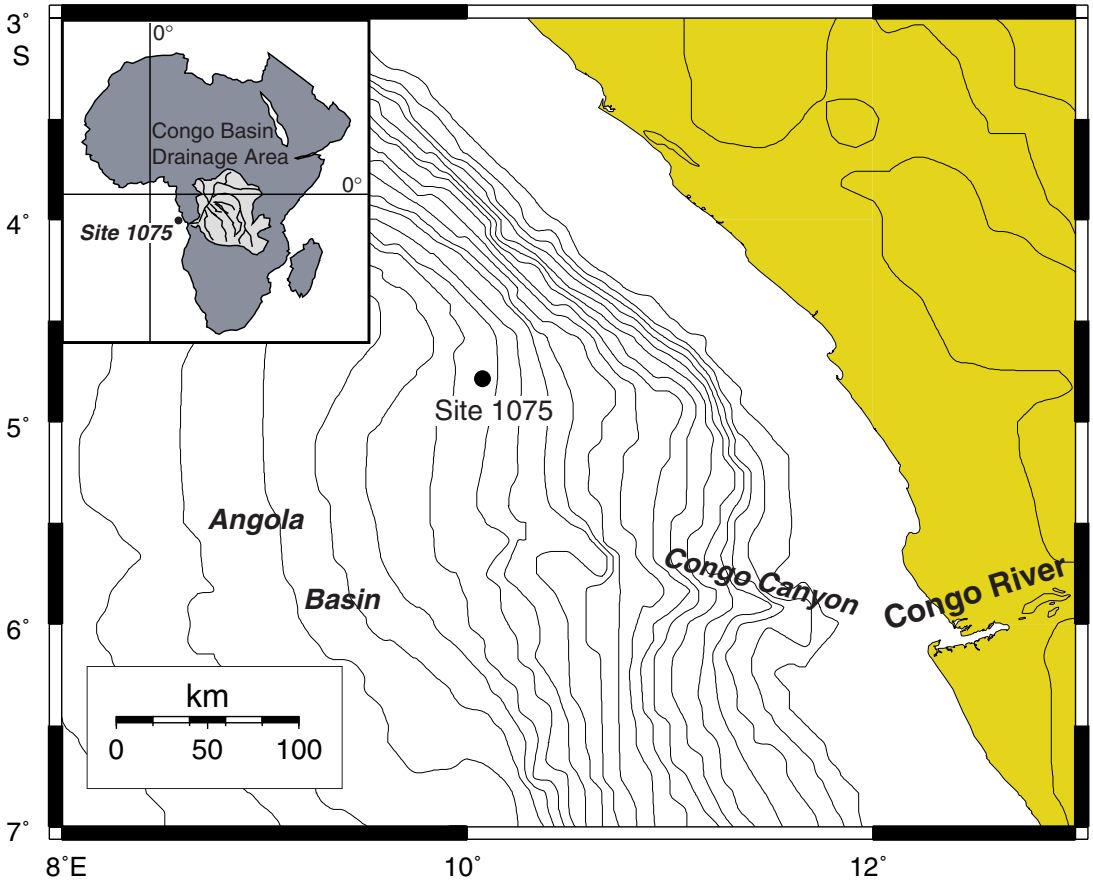

Figure F2. The susceptibility record of the composite section at Site 1075. Shaded intervals were selected for detailed rock-magnetic and geochemical measurements.

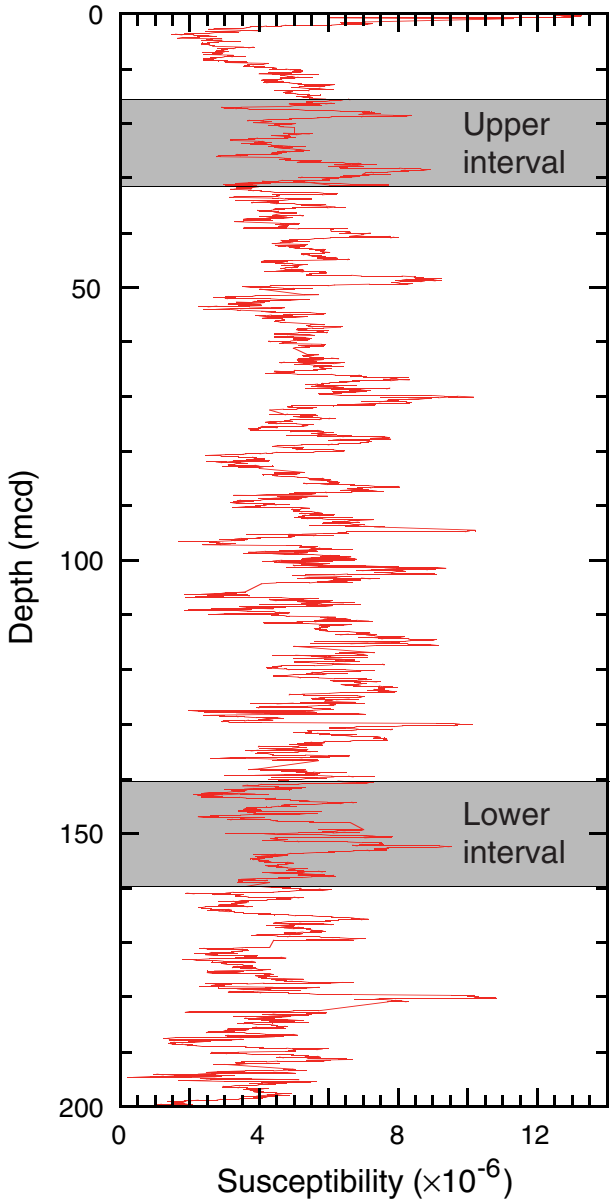

Figure F3. Low-temperature demagnetizations of an IRM (3 T) show no evidence for phase transitions characteristic of magnetic carrier minerals. The strong intensity decay between 20 and 50 K is caused by clay minerals.

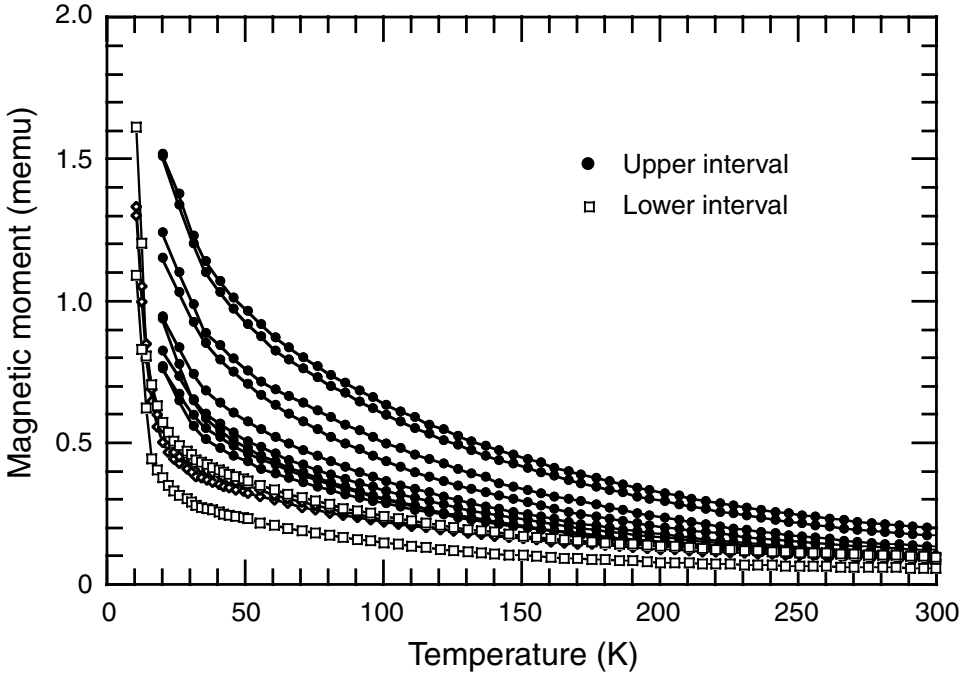

Figure F4. Hysteresis measurements of two samples (**A**, **C**) before and (**B**, **D**) after high-field slope correction.

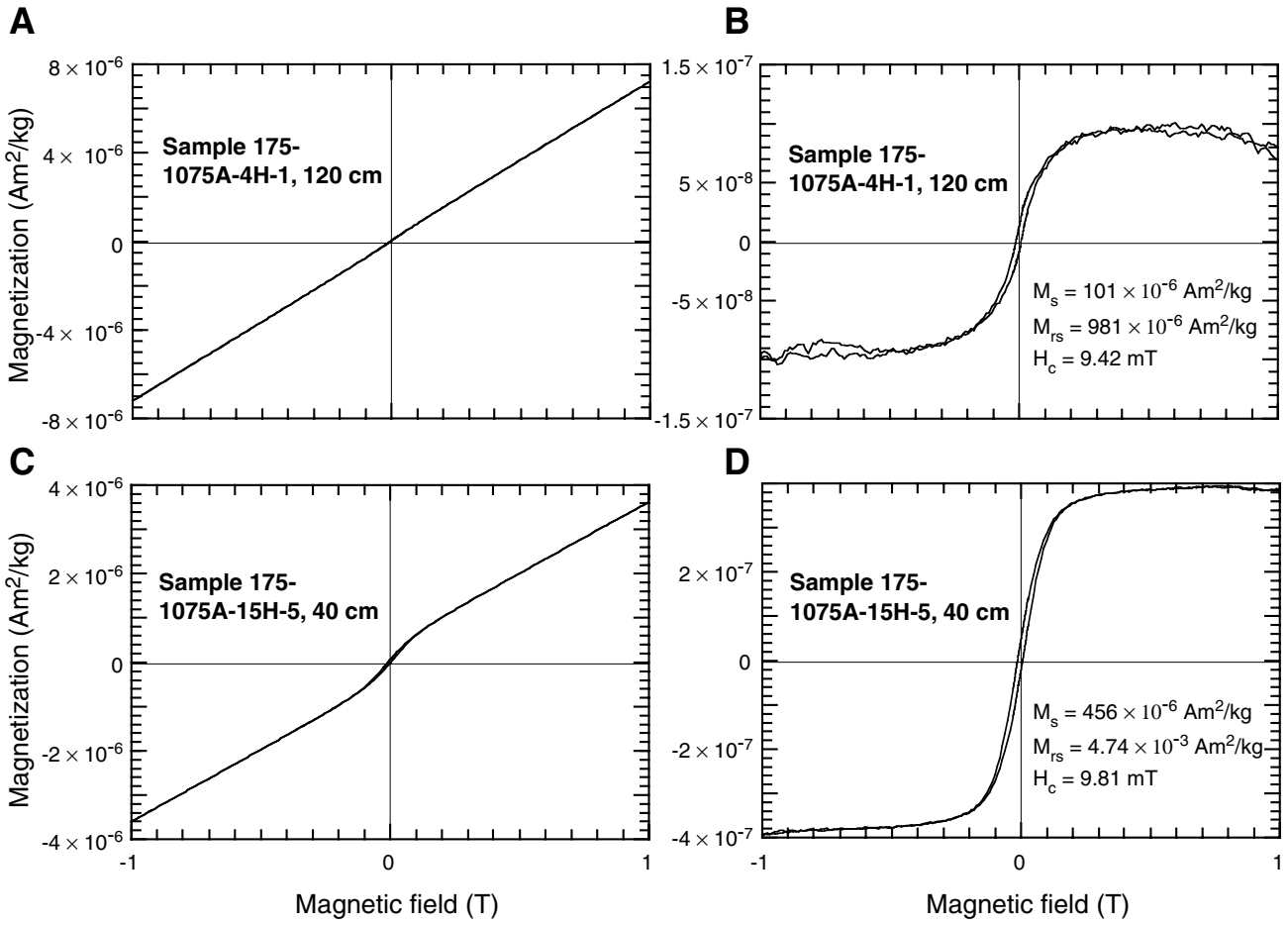

Figure F5. Partial ARM (pARM) acquisition curves have a maximum at a 10–20 mT biasing field (up arrow), indicating a mean magnetic grain size of 3–5 µm (Jackson et al., 1988). The scatter in the (**A**) upper interval is significantly larger than in the (**B**) lower interval.

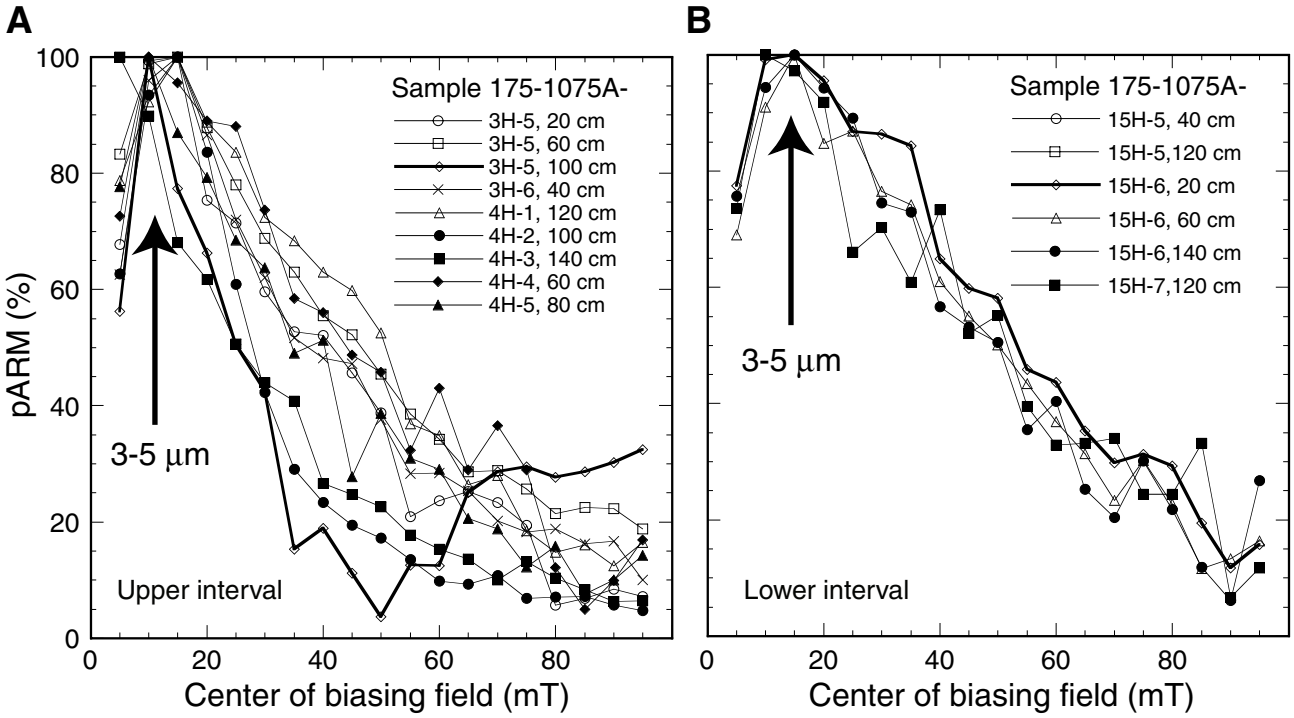

Figure F6. Rock-magnetic properties of the two investigated depth intervals (top panel = upper interval; bottom panel = lower interval). Horizontal shaded boxes highlight high values of shipboard susceptibility values (far left panel) for comparison.

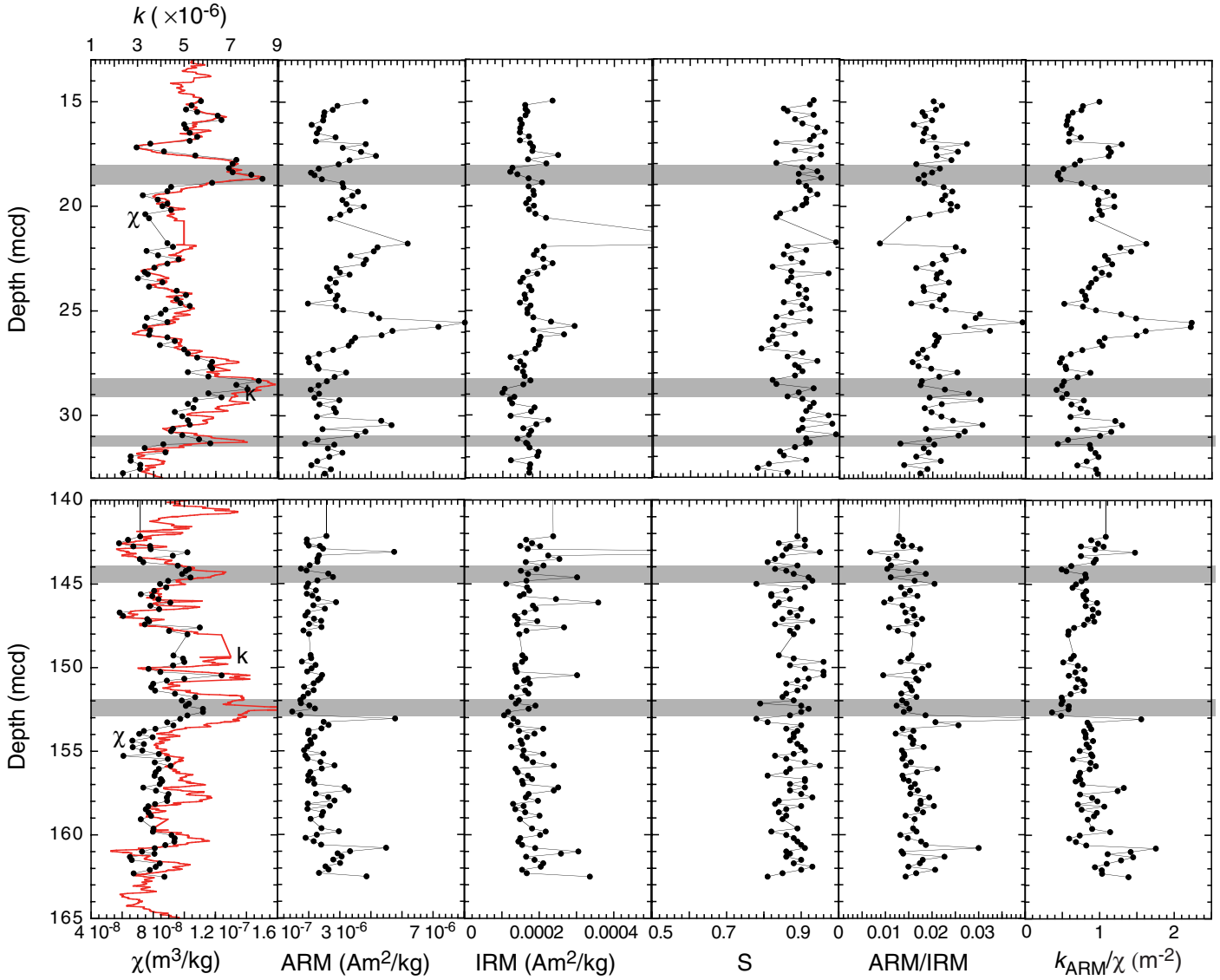

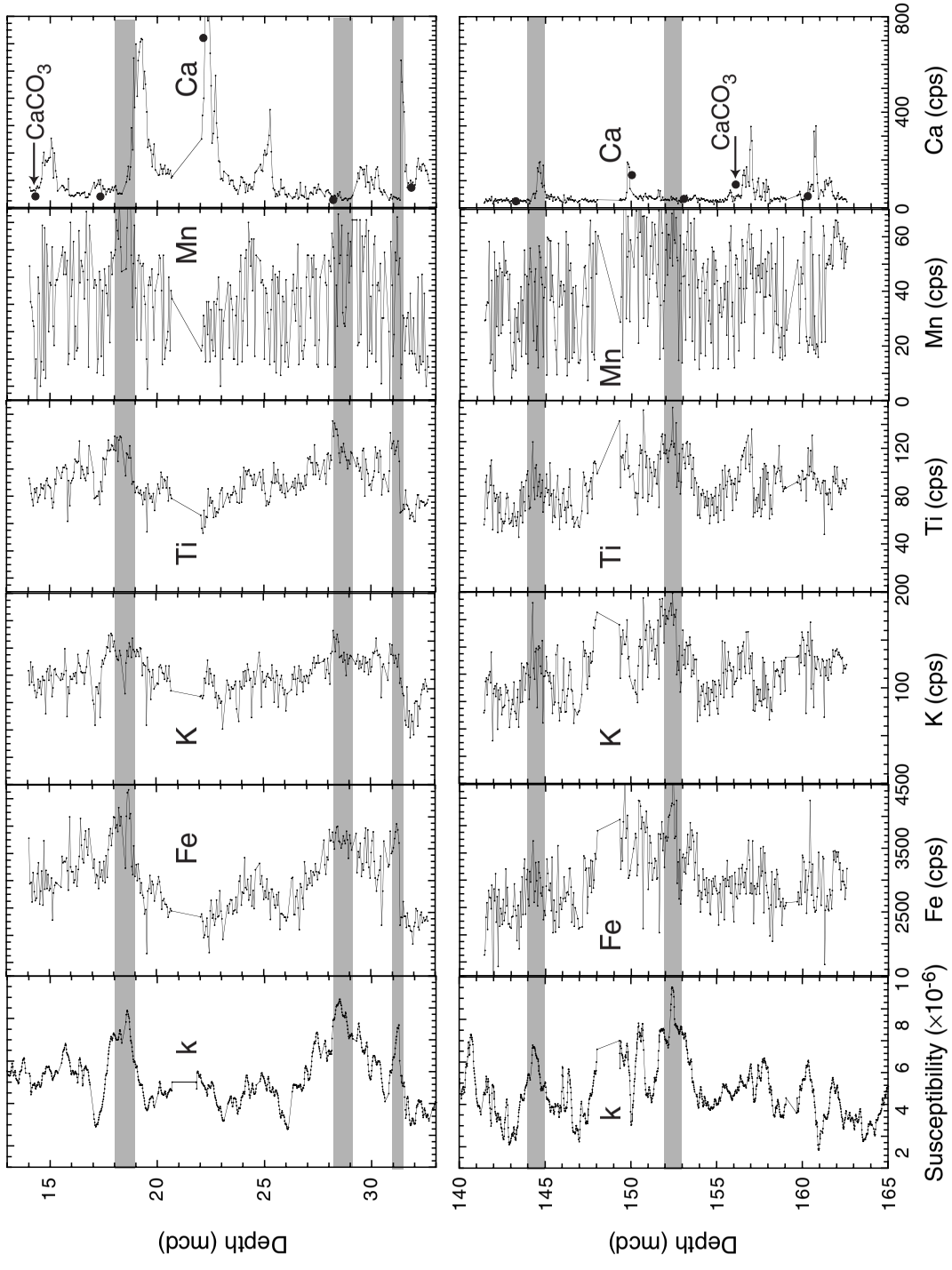

Figure F7. XRF core-scanner data of the upper (top panel) and lower (bottom panel) intervals. Magnetic susceptibility data (far left panel) are shown for comparison. Horizontal shaded boxes highlight high values of shipboard susceptibility values (far left panel) for comparison.

Table T1. Rock-magnetic data, Site 1075. (See table notes. Continued on next three pages).

Core, section, interval (cm)	Depth (mbsf)	Depth (mcd)	χ (m^3/kg)	ARM (Am^2/kg)	k_{ARM} (m/kg)	IRM (Am^2/kg)	BIRM (Am^2/kg)	S-ratio
175-1075A-								
3H-3, 98-100	14.98	14.98	1.1949E–07	4.7164E–06	1.1850E–07	0.000233	0.000218	0.93
3H-3, 118-120	15.18	15.18	1.1445E–07	3.5169E–06	8.8365E–08	0.000160	0.000147	0.92
3H-3, 138-140	15.38	15.38	1.1081E–07	3.3163E–06	8.3324E–08	0.000161	0.000137	0.85
3H-4, 0-2	15.50	15.50	1.1713E–07	2.9560E–06	7.4272E–08	0.000166	0.000144	0.86
3H-4, 18-20	15.68	15.68	1.2809E–07	2.9397E–06	7.3861E–08	0.000161	0.000150	0.93
3H-4, 38-40	15.88	15.88	1.2966E–07	2.9148E–06	7.3237E–08	0.000147	0.000129	0.88
3H-4, 58-60	16.08	16.08	1.1005E–07	2.4175E–06	6.0740E–08	0.000151	0.000136	0.90
3H-4, 78-80	16.28	16.28	1.1082E–07	2.7315E–06	6.8631E–08	0.000147	0.000138	0.94
3H-4, 98-100	16.48	16.48	1.1295E–07	2.6498E–06	6.6577E–08	0.000146	0.000140	0.96
3H-4, 118-120	16.68	16.68	1.1668E–07	3.4447E–06	8.6551E–08	0.000170	0.000158	0.93
3H-4, 138-140	16.88	16.88	1.1281E–07	2.6144E–06	6.5689E–08	0.000146	0.000135	0.92
3H-5, 0-2	17.00	17.00	9.1883E–08	4.7343E–06	1.1895E–07	0.000173	0.000143	0.83
3H-5, 18-20	17.18	17.18	8.4501E–08	3.7463E–06	9.4129E–08	0.000181	0.000171	0.95
3H-5, 38-40	17.38	17.38	9.9287E–08	4.5401E–06	1.1407E–07	0.000179	0.000158	0.88
3H-5, 58-60	17.58	17.58	1.1612E–07	5.1739E–06	1.3000E–07	0.000248	0.000235	0.95
3H-5, 78-80	17.78	17.78	1.3816E–07	4.0448E–06	1.0163E–07	0.000168	0.000155	0.92
3H-5, 98-100	17.98	17.98	1.3575E–07	3.5754E–06	8.9834E–08	0.000217	0.000181	0.83
3H-5, 118-120	18.18	18.18	1.3406E–07	2.7184E–06	6.8302E–08	0.000126	0.000114	0.90
3H-5, 138-140	18.38	18.38	1.3589E–07	2.3868E–06	5.9970E–08	0.000120	0.000113	0.94
3H-6, 0-2	18.50	18.50	1.4614E–07	2.5257E–06	6.3459E–08	0.000139	0.000124	0.89
3H-6, 18-20	18.68	18.68	1.5196E–07	2.8577E–06	7.1802E–08	0.000169	0.000161	0.95
3H-6, 38-40	18.88	18.88	1.2522E–07	3.7347E–06	9.3837E–08	0.000205	0.000182	0.89
3H-6, 58-60	19.08	19.08	1.0263E–07	3.7729E–06	9.4798E–08	0.000169	0.000153	0.91
3H-6, 78-80	19.28	19.28	1.0061E–07	4.3962E–06	1.1046E–07	0.000182	0.000167	0.92
3H-6, 98-100	19.48	19.48	8.7946E–08	4.1645E–06	1.0464E–07	0.000184	0.000172	0.94
3H-6, 118-120	19.68	19.68	9.5811E–08	3.7411E–06	9.3996E–08	0.000170	0.000155	0.91
3H-6, 138-140	19.88	19.88	1.0057E–07	3.8990E–06	9.7965E–08	0.000163	0.000149	0.91
3H-7, 0-2	20.00	20.00	9.8360E–08	4.6638E–06	1.1718E–07	0.000184	0.000165	0.90
3H-7, 18-20	20.18	20.18	1.0279E–07	4.0571E–06	1.0194E–07	0.000170	0.000149	0.88
3H-7, 38-40	20.38	20.38	8.9341E–08	3.6429E–06	9.1531E–08	0.000188	0.000159	0.84
3H-7, 58-60	20.58	20.58	9.1211E–08	3.2173E–06	8.0835E–08	0.000216	0.000180	0.83
4H-1, 0-2	20.50	21.76	1.0112E–07	6.5285E–06	1.6403E–07	0.000754	0.000746	0.99
4H-1, 18-20	20.68	21.94	1.0360E–07	5.2356E–06	1.3155E–07	0.000210	0.000180	0.86
4H-1, 38-40	20.88	22.14	8.9837E–08	5.0777E–06	1.2758E–07	0.000191	0.000174	0.91
4H-1, 58-60	21.08	22.34	9.5953E–08	4.0829E–06	1.0259E–07	0.000184	0.000155	0.85
4H-1, 78-80	21.28	22.54	1.0733E–07	4.7465E–06	1.1926E–07	0.000208	0.000182	0.87
4H-1 98-100	21.48	22.74	1.0063E–07	4.6541E–06	1.1694E–07	0.000233	0.000210	0.90
4H-1, 118-120	21.68	22.94	9.4049E–08	3.4752E–06	8.7316E–08	0.000211	0.000172	0.82
4H-1, 138-140	21.88	23.14	8.8782E–08	3.6307E–06	9.1223E–08	0.000167	0.000145	0.87
4H-2, 0-2	22.00	23.26	9.0517E–08	4.0354E–06	1.0139E–07	0.000193	0.000187	0.97
4H-2,18-20	22.18	23.44	8.5218E–08	3.2088E–06	8.0623E–08	0.000154	0.000135	0.87
4H-2, 38-40	22.38	23.64	9.8366E–08	3.4557E–06	8.6825E–08	0.000147	0.000127	0.86
4H-2, 58-60	22.58	23.84	9.1171E–08	3.0806E–06	7.7402E–08	0.000171	0.000153	0.89
4H-2, 78-80	22.78	24.04	1.0582E–07	3.2006E–06	8.0416E–08	0.000177	0.000160	0.91
4H-2, 98-100	22.98	24.24	1.1068E–07	3.5216E–06	8.8483E–08	0.000158	0.000141	0.89
4H-2, 118-120	23.18	24.44	1.0643E–07	3.4519E–06	8.6730E–08	0.000161	0.000147	0.91
4H-2, 138-140	23.38	24.64	1.0845E–07	2.2527E–06	5.6600E–08	0.000146	0.000124	0.85
4H-3, 0-2	23.50	24.76	1.1265E–07	3.4667E–06	8.7103E–08	0.000174	0.000156	0.90
4H-3, 18-20	23.68	24.94	1.0039E–07	3.7800E–06	9.4975E–08	0.000166	0.000152	0.92
4H-3, 38-40	23.88	25.14	9.7541E–08	4.9900E–06	1.2538E–07	0.000166	0.000144	0.87
4H-3, 58-60	24.08	25.34	8.9976E–08	5.3142E–06	1.3352E–07	0.000182	0.000151	0.83
4H-3, 78-80	24.28	25.54	1.0130E–07	8.9866E–06	2.2579E–07	0.000229	0.000211	0.92
4H-3, 98-100	24.48	25.74	8.9030E–08	7.8610E–06	1.9751E–07	0.000293	0.000248	0.85
4H-3, 118-120	24.68	25.94	9.1584E–08	5.8797E–06	1.4773E–07	0.000182	0.000150	0.82
4H-3, 138-140	24.88	26.14	9.1169E–08	5.4185E–06	1.3614E–07	0.000264	0.000232	0.88
4H-4, 0-2	25.00	26.26	1.0118E–07	4.2805E–06	1.0755E–07	0.000201	0.000164	0.82
4H-4, 18-20	25.18	26.44	1.0502E–07	4.1424E–06	1.0408E–07	0.000198	0.000161	0.81
4H-4, 38-40	25.38	26.64	9.6965E–08	3.9982E–06	1.0046E–07	0.000196	0.000163	0.83
4H-4, 58-60	25.58	26.84	1.1035E–07	3.3418E–06	8.3964E–08	0.000187	0.000147	0.79
4H-4, 78-80	25.78	27.04	1.1236E–07	2.7277E–06	6.8536E–08	0.000162	0.000145	0.90
4H-4, 98-100	25.98	27.24	1.1677E–07	2.2718E–06	5.7080E–08	0.000121	0.000104	0.86
4H-4, 118-120	26.18	27.44	1.2510E–07	2.3066E–06	5.7954E–08	0.000147	0.000138	0.94
4H-4, 138-140	26.38	27.64	1.2412E–07	2.6594E–06	6.6819E–08	0.000157	0.000139	0.88
4H-5, 0-2	26.50	27.76	1.2497E–07	2.7116E–06	6.8130E–08	0.000138	0.000123	0.89
4H-5, 18-20	26.68	27.94	1.1210E–07	3.8911E–06	9.7766E–08	0.000154	0.000138	0.90
4H-5, 38-40	26.88	28.14	1.2278E–07	3.4114E–06	8.5713E–08	0.000159	0.000139	0.88
4H-5, 58-60	27.08	28.34	1.4960E–07	3.0712E–06	7.7166E–08	0.000174	0.000143	0.82

Table T1 (continued).

Core, section, interval (cm)	Depth (mbsf)	Depth (mcd)	χ (m^3/kg)	ARM (Am^2/kg)	k_{ARM} (m/kg)	IRM (Am^2/kg)	BIRM (Am^2/kg)	S-ratio
4H-5, 78-80	27.28	28.54	1.3822E–07	2.6994E–06	6.7823E–08	0.000155	0.000129	0.83
4H-5, 98-100	27.48	28.74	1.4424E–07	2.3837E–06	5.9891E–08	0.000105	0.000098	0.93
4H-5, 118-120	27.68	28.94	1.2346E–07	2.7363E–06	6.8751E–08	0.000099	0.000087	0.89
4H-5, 138-140	27.88	29.14	1.2994E–07	2.5352E–06	6.3699E–08	0.000131	0.000112	0.86
4H-6, 0-2	28.00	29.26	1.1575E–07	3.6128E–06	9.0774E–08	0.000119	0.000108	0.90
4H-6, 18-20	28.18	29.44	1.1156E–07	2.7491E–06	6.9074E–08	0.000125	0.000116	0.93
4H-6, 38-40	28.38	29.64	1.1495E–07	3.3844E–06	8.5035E–08	0.000185	0.000170	0.92
4H-6, 58-60	28.58	29.84	1.0504E–07	3.4633E–06	8.7017E–08	0.000176	0.000160	0.91
4H-6, 78-80	28.78	30.04	1.0933E–07	2.6430E–06	6.6406E–08	0.000121	0.000117	0.97
4H-6, 98-100	28.98	30.24	1.1250E–07	5.3971E–06	1.3561E–07	0.000222	0.000199	0.90
4H-6, 118-120	29.18	30.44	1.1310E–07	5.8359E–06	1.4663E–07	0.000190	0.000186	0.98
4H-6, 138-140	29.38	30.64	1.0419E–07	2.8817E–06	7.2406E–08	0.000155	0.000141	0.90
4H-7, 0-2	29.50	30.76	1.0308E–07	4.7234E–06	1.1868E–07	0.000176	0.000156	0.89
4H-7, 18-20	29.68	30.94	1.0903E–07	4.3461E–06	1.0920E–07	0.000170	0.000169	0.99
4H-7, 38-40	29.88	31.14	1.1754E–07	2.6667E–06	6.7002E–08	0.000139	0.000125	0.91
4H-7, 58-60	30.08	31.34	1.2356E–07	2.1294E–06	5.3503E–08	0.000163	0.000151	0.92
5H-1, 0-2	30.00	30.68	9.8832E–08	3.3872E–06	8.5107E–08	0.000166	0.000152	0.91
5H-1, 18-20	30.18	30.86	8.8912E–08	3.1067E–06	7.8058E–08	0.000172	0.000151	0.88
5H-1, 38-40	30.38	31.06	1.0002E–07	3.7424E–06	9.4031E–08	0.000196	0.000164	0.84
5H-1, 58-60	30.58	31.26	8.1420E–08	3.1822E–06	7.9954E–08	0.000193	0.000164	0.85
5H-1, 78-80	30.78	31.46	8.1353E–08	2.6568E–06	6.6754E–08	0.000122	0.000111	0.91
5H-1, 98-100	30.98	31.66	8.6505E–08	2.3952E–06	6.0182E–08	0.000173	0.000140	0.81
5H-1, 118-120	31.18	31.86	8.6376E–08	3.2470E–06	8.1582E–08	0.000172	0.000134	0.78
5H-1, 138-140	31.38	32.06	7.7235E–08	2.9716E–06	7.4663E–08	0.000171	0.000148	0.86
15H-4, 78-80	128.96	142.17	7.1579E–08	3.0900E–06	7.7639E–08	0.000238	0.000211	0.89
15H-4, 98-100	129.16	142.37	6.3870E–08	2.2584E–06	5.6744E–08	0.000165	0.000150	0.91
15H-4, 118-120	129.36	142.57	5.7971E–08	2.2573E–06	5.6715E–08	0.000181	0.000152	0.84
15H-4, 138-140	129.56	142.77	6.7199E–08	2.8190E–06	7.0829E–08	0.000203	0.000178	0.88
15H-5, 0-2	129.53	142.74	7.7973E–08	2.3315E–06	5.8581E–08	0.000149	0.000135	0.91
15H-5, 18-20	129.71	142.92	7.8410E–08	2.9460E–06	7.4021E–08	0.000169	0.000145	0.86
15H-5, 38-40	129.91	143.12	1.0219E–07	5.9959E–06	1.5065E–07	0.000888	0.000841	0.95
15H-5, 58-60	130.11	143.32	9.2708E–08	2.7775E–06	6.9786E–08	0.000224	0.000191	0.85
15H-5, 78-80	130.31	143.52	7.1385E–08	2.7036E–06	6.7929E–08	0.000254	0.000212	0.83
15H-5, 98-100	130.51	143.72	7.3610E–08	2.6990E–06	6.7815E–08	0.000164	0.000133	0.81
15H-5, 118-120	130.71	143.92	9.5838E–08	2.3731E–06	5.9626E–08	0.000212	0.000189	0.89
15H-5, 138-140	130.91	144.12	1.0286E–07	2.0119E–06	5.0549E–08	0.000193	0.000161	0.83
15H-6, 0-2	131.03	144.24	1.0144E–07	2.2383E–06	5.6237E–08	0.000151	0.000130	0.86
15H-6, 18-20	131.21	144.42	9.8460E–08	3.1696E–06	7.9638E–08	0.000170	0.000149	0.88
15H-6, 38-40	131.41	144.62	1.0372E–07	3.3719E–06	8.4720E–08	0.000302	0.000277	0.92
15H-6, 58-60	131.61	144.82	8.9632E–08	2.7061E–06	6.7993E–08	0.000166	0.000154	0.93
15H-6, 78-80	131.81	145.02	8.4441E–08	2.3006E–06	5.7804E–08	0.000112	0.000087	0.78
15H-6, 98-100	132.01	145.22	8.8409E–08	2.2386E–06	5.6247E–08	0.000168	0.000153	0.91
15H-6, 118-120	132.21	145.42	8.0690E–08	2.6411E–06	6.6360E–08	0.000173	0.000148	0.86
15H-6, 138-140	132.41	145.62	7.2019E–08	2.2515E–06	5.6571E–08	0.000159	0.000131	0.82
15H-7, 0-2	132.53	145.74	7.9405E–08	2.4937E–06	6.2655E–08	0.000148	0.000121	0.82
15H-7, 18-20	132.71	145.92	8.3547E–08	2.7255E–06	6.8480E–08	0.000245	0.000213	0.87
15H-7, 38-40	132.91	146.12	9.0972E–08	3.4969E–06	8.7861E–08	0.000359	0.000301	0.84
15H-7, 58-60	133.11	146.32	7.8274E–08	2.5277E–06	6.3510E–08	0.000184	0.000153	0.83
15H-7, 78-80	133.31	146.52	8.3781E–08	3.0275E–06	7.6069E–08	0.000191	0.000171	0.90
15H-7, 98-100	133.51	146.72	5.8503E–08	2.2948E–06	5.7658E–08	0.000161	0.000140	0.87
15H-7, 118-120	133.71	146.92	6.0568E–08	2.1872E–06	5.4954E–08	0.000135	0.000119	0.89
15H-7, 138-140	133.91	147.12	7.6254E–08	2.5597E–06	6.4313E–08	0.000143	0.000123	0.85
15H-8, 0-2	134.03	147.24	7.7519E–08	2.8734E–06	7.2196E–08	0.000195	0.000182	0.93
15H-8, 18-20	134.21	147.42	7.4646E–08	2.3476E–06	5.8986E–08	0.000141	0.000118	0.83
15H-8, 38-40	134.41	147.62	1.1030E–07	2.8833E–06	7.2445E–08	0.000267	0.000237	0.89
15H-8, 58-60	134.61	147.82	9.0177E–08	2.1005E–06	5.2776E–08	0.000166	0.000145	0.87
15H-8, 78-80	134.81	148.02	1.0179E–07	2.3484E–06	5.9005E–08	0.000147	0.000130	0.88
16H-1, 0-2	134.50	149.29	9.3086E–08	2.4202E–06	6.0810E–08	0.000155	0.000130	0.84
16H-1, 18-20	134.68	149.47	9.9301E–08	2.4379E–06	6.1254E–08	0.000163	0.000143	0.88
16H-1, 38-40	134.88	149.67	1.0036E–07	2.0462E–06	5.1413E–08	0.000154	0.000148	0.96
16H-1, 58-60	135.08	149.87	9.2854E–08	2.6293E–06	6.6063E–08	0.000136	0.000119	0.87
16H-1, 78-80	135.28	150.07	7.6962E–08	2.4520E–06	6.1609E–08	0.000137	0.000125	0.91
16H-1, 98-100	135.48	150.27	8.4597E–08	2.2697E–06	5.7027E–08	0.000140	0.000134	0.96
16H-1, 118-120	135.68	150.47	1.2373E–07	2.8970E–06	7.2788E–08	0.000302	0.000292	0.96
16H-1, 138-140	135.88	150.67	1.0002E–07	2.8330E–06	7.1181E–08	0.000170	0.000157	0.92
16H-2, 0-2	136.00	150.79	8.8756E–08	2.7397E–06	6.8836E–08	0.000160	0.000143	0.89
16H-2, 18-20	136.18	150.97	7.9997E–08	2.5478E–06	6.4014E–08	0.000175	0.000151	0.86
16H-2, 38-40	136.38	151.17	7.8806E–08	2.1429E–06	5.3841E–08	0.000140	0.000127	0.91
16H-2, 58-60	136.58	151.37	8.1262E–08	2.5481E–06	6.4023E–08	0.000163	0.000145	0.89

Table T1 (continued).

Core, section, interval (cm)	Depth (mbsf)	Depth (mcd)	χ (m^3/kg)	ARM (Am^2/kg)	k_{ARM} (m/kg)	IRM (Am^2/kg)	BIRM (Am^2/kg)	S-ratio
16H-2, 78-80	136.78	151.57	9.4080E–08	2.3001E–06	5.7791E–08	0.000171	0.000148	0.86
16H-2, 98-100	136.98	151.77	1.0711E–07	2.1005E–06	5.2776E–08	0.000126	0.000107	0.85
16H-2, 118-120	137.18	151.97	9.8376E–08	1.9804E–06	4.9760E–08	0.000145	0.000129	0.88
16H-2, 138-140	137.38	152.17	1.0338E–07	2.0115E–06	5.0541E–08	0.000138	0.000109	0.79
16H-3, 0-2	137.50	152.29	1.0055E–07	2.3615E–06	5.9335E–08	0.000190	0.000170	0.90
16H-3, 18-20	137.68	152.47	1.1219E–07	2.6134E–06	6.5664E–08	0.000172	0.000158	0.92
16H-3, 38-40	137.88	152.67	1.1217E–07	1.6250E–06	4.0830E–08	0.000117	0.000105	0.90
16H-3, 58-60	138.08	152.87	1.0180E–07	1.9678E–06	4.9442E–08	0.000106	0.000092	0.87
16H-3, 78-80	138.28	153.07	9.7449E–08	6.0407E–06	1.5178E–07	0.000131	0.000102	0.78
16H-3, 98-100	138.48	153.27	8.9069E–08	2.9669E–06	7.4546E–08	0.000143	0.000116	0.81
16H-3, 118-120	138.68	153.47	9.3085E–08	3.1925E–06	8.0215E–08	0.000124	0.000112	0.90
16H-3, 138-140	138.88	153.67	8.1368E–08	2.8773E–06	7.2295E–08	0.000211	0.000181	0.86
16H-4, 0-2	139.00	153.79	7.4002E–08	2.3316E–06	5.8583E–08	0.000146	0.000130	0.89
16H-4, 18-20	139.18	153.97	7.0995E–08	2.2977E–06	5.7730E–08	0.000188	0.000165	0.88
16H-4, 38-40	139.38	154.17	7.9719E–08	2.5877E–06	6.5018E–08	0.000168	0.000147	0.88
16H-4, 58-60	139.58	154.37	6.6462E–08	2.4116E–06	6.0593E–08	0.000150	0.000131	0.87
16H-4, 78-80	139.78	154.57	7.4083E–08	2.4387E–06	6.1275E–08	0.000154	0.000137	0.89
16H-4, 98-100	139.98	154.77	6.6839E–08	2.2827E–06	5.7354E–08	0.000125	0.000113	0.90
16H-4, 118-120	140.18	154.97	7.3059E–08	2.1326E–06	5.3583E–08	0.000158	0.000144	0.91
16H-4, 138-140	140.38	155.17	8.3564E–08	2.9592E–06	7.4351E–08	0.000211	0.000186	0.88
16H-5, 0-2	140.50	155.29	6.0767E–08	2.1902E–06	5.5029E–08	0.000156	0.000129	0.83
16H-5, 18-20	140.68	155.47	8.9410E–08	2.2804E–06	5.7297E–08	0.000166	0.000144	0.86
16H-5, 38-40	140.88	155.67	8.1074E–08	2.8393E–06	7.1339E–08	0.000183	0.000167	0.91
16H-5, 58-60	141.08	155.87	9.1285E–08	3.4496E–06	8.6673E–08	0.000239	0.000228	0.95
16H-5, 78-80	141.28	156.07	8.3630E–08	2.8941E–06	7.2717E–08	0.000137	0.000119	0.87
16H-5, 98-100	141.48	156.27	8.1626E–08	2.3988E–06	6.0271E–08	0.000143	0.000123	0.86
16H-5, 118-120	141.68	156.47	8.0877E–08	2.3167E–06	5.8208E–08	0.000170	0.000138	0.81
16H-5, 138-140	141.88	156.67	8.5001E–08	2.5162E–06	6.3222E–08	0.000181	0.000164	0.91
16H-6, 0-2	142.00	156.79	8.5755E–08	2.3122E–06	5.8096E–08	0.000154	0.000141	0.91
16H-6, 18-20	142.18	156.97	8.4196E–08	2.5783E–06	6.4782E–08	0.000157	0.000137	0.87
16H-6, 38-40	142.38	157.17	7.3732E–08	3.8832E–06	9.7568E–08	0.000251	0.000229	0.91
16H-6, 58-60	142.58	157.37	8.1781E–08	4.0503E–06	1.0177E–07	0.000239	0.000208	0.87
16H-6, 78-80	142.78	157.57	8.9764E–08	2.6372E–06	6.6261E–08	0.000172	0.000154	0.90
16H-6, 98-100	142.98	157.77	8.8760E–08	3.1846E–06	8.0015E–08	0.000164	0.000152	0.93
16H-6, 118-120	143.18	157.97	8.9051E–08	3.4518E–06	8.6728E–08	0.000197	0.000165	0.84
16H-6, 138-140	143.38	158.17	8.1189E–08	2.2874E–06	5.7473E–08	0.000130	0.000108	0.83
16H-7, 0-2	143.50	158.29	7.6790E–08	3.2502E–06	8.1663E–08	0.000159	0.000143	0.90
16H-7, 18-20	143.68	158.47	7.5274E–08	2.2772E–06	5.7217E–08	0.000136	0.000116	0.86
16H-7, 38-40	143.88	158.67	7.7034E–08	2.9504E–06	7.4130E–08	0.000163	0.000138	0.84
16H-7, 58-60	144.08	158.87	7.8687E–08	2.8934E–06	7.2699E–08	0.000201	0.000173	0.86
16H-7, 78-80	144.28	159.07	7.2015E–08	2.4174E–06	6.0738E–08	0.000148	0.000126	0.85
17H-1, 0-2	144.00	159.63	8.0292E–08	2.8761E–06	7.2263E–08	0.000181	0.000160	0.89
17H-1, 18-20	144.18	159.81	7.9763E–08	3.6311E–06	9.1234E–08	0.000218	0.000179	0.82
17H-1, 38-40	144.38	160.01	9.1935E–08	2.6838E–06	6.7432E–08	0.000203	0.000175	0.86
17H-1, 58-60	144.58	160.21	9.3865E–08	2.2082E–06	5.5483E–08	0.000149	0.000132	0.88
17H-1, 78-80	144.78	160.41	9.3709E–08	2.5483E–06	6.4027E–08	0.000144	0.000128	0.89
17H-1, 98-100	144.98	160.61	8.7943E–08	2.8728E–06	7.2181E–08	0.000154	0.000139	0.90
17H-1, 118-120	145.18	160.81	8.1115E–08	5.6615E–06	1.4225E–07	0.000189	0.000172	0.91
17H-1, 138-140	145.38	161.01	7.2827E–08	4.1056E–06	1.0316E–07	0.000305	0.000262	0.86
17H-2, 0-2	145.50	161.13	8.0886E–08	3.5714E–06	8.9734E–08	0.000259	0.000224	0.87
17H-2, 18-20	145.68	161.31	6.5058E–08	3.7544E–06	9.4332E–08	0.000165	0.000142	0.86
17H-2, 38-40	145.88	161.51	6.6210E–08	3.3942E–06	8.5282E–08	0.000188	0.000170	0.90
17H-2, 58-60	146.08	161.71	8.4235E–08	3.6760E–06	9.2362E–08	0.000211	0.000186	0.88
17H-2, 78-80	146.28	161.91	8.1628E–08	3.0460E–06	7.6534E–08	0.000204	0.000189	0.93
17H-2, 98-100	146.48	162.11	7.7949E–08	3.1941E–06	8.0254E–08	0.000154	0.000139	0.90
17H-2, 118-120	146.68	162.31	6.7435E–08	2.7740E–06	6.9699E–08	0.000167	0.000142	0.85
17H-2, 138-140B	146.88	162.51	8.7169E–08	4.8204E–06	1.2112E–07	0.000336	0.000273	0.81
175-1075B-								
3H-4, 0-2	19.00	20.38	9.9979E–08	4.7316E–06	1.1889E–07	0.000237	0.000198	0.84
3H-4, 18-20	19.18	20.56	9.5527E–08	4.8448E–06	1.2173E–07	0.000223	0.000195	0.87
3H-4, 38-40	19.38	20.76	8.7111E–08	3.2817E–06	8.2455E–08	0.000159	0.000143	0.90
3H-4, 58-60	19.58	20.96	1.0045E–07	6.0534E–06	1.5210E–07	0.000280	0.000258	0.92
3H-4, 78-80	19.78	21.16	1.0679E–07	3.1420E–06	7.8944E–08	0.000167	0.000132	0.79
3H-4, 98-100	19.98	21.36	1.0086E–07	3.4391E–06	8.6409E–08	0.000177	0.000150	0.85
3H-4, 118-120	20.18	21.56	9.7865E–08	3.5056E–06	8.8082E–08	0.000179	0.000156	0.87
3H-4, 138-140	20.38	21.76	9.4587E–08	4.2439E–06	1.0663E–07	0.000281	0.000255	0.91
15H-6, 58-60	135.39	147.85	8.8174E–08	2.7911E–06	7.0127E–08	0.000209	0.000190	0.91
15H-6, 78-80	135.59	148.05	1.0186E–07	2.5068E–06	6.2985E–08	0.000121	0.000102	0.84
15H-6, 98-100	135.79	148.25	9.4199E–08	2.1568E–06	5.4192E–08	0.000143	0.000115	0.80

Table T1 (continued).

Core, section, interval (cm)	Depth (mbsf)	Depth (mcd)	χ (m^3/kg)	ARM (Am^2/kg)	k_{ARM} (m/kg)	IRM (Am^2/kg)	BIRM (Am^2/kg)	S-ratio
15H-6, 118-120	135.99	148.45	9.2521E–08	2.0837E–06	5.2353E–08	0.000124	0.000112	0.90
15H-6, 138-140	136.19	148.65	8.5757E–08	3.4452E–06	8.6563E–08	0.000147	0.000123	0.84
15H-7, 0-2	136.31	148.77	8.9367E–08	2.7866E–06	7.0016E–08	0.000158	0.000133	0.84
15H-7, 18-20	136.49	148.95	1.0209E–07	2.7316E–06	6.8632E–08	0.000155	0.000136	0.88
15H-7, 38-40	136.69	149.15	9.6477E–08	2.1359E–06	5.3666E–08	0.000145	0.000119	0.82
15H-7, 58-60	136.89	149.35	9.4130E–08	2.0259E–06	5.0902E–08	0.000136	0.000099	0.73
16H-6, 0-2	144.15	158.45	8.6020E–08	3.9216E–06	9.8532E–08	0.000189	0.000162	0.85
16H-6, 18-20	144.33	158.63	8.7463E–08	3.9762E–06	9.9904E–08	0.000283	0.000252	0.89
16H-6, 38-40	144.53	158.83	7.0305E–08	2.8559E–06	7.1756E–08	0.000164	0.000150	0.91
16H-6, 58-60	144.73	159.03	7.3815E–08	2.9643E–06	7.4479E–08	0.000200	0.000176	0.88
16H-6, 78-80	144.93	159.23	6.9039E–08	2.4759E–06	6.2208E–08	0.000174	0.000156	0.90
16H-6, 98-100	145.13	159.43	7.8181E–08	2.2260E–06	5.5930E–08	0.000142	0.000120	0.85
16H-6	145.33	159.63	8.0498E–08	2.4771E–06	6.2240E–08	0.000137	0.000116	0.85
16H-6	145.53	159.83	7.4223E–08	2.4493E–06	6.1541E–08	0.000124	0.000109	0.88

Notes: χ = mass-specific magnetic susceptibility, ARM = anhysteric remanent magnetization, k_{ARM} = susceptibility of ARM, IRM = isothermal remanent magnetization, BIRM = backfield isothermal remanent magnetization. S-ratio = IRM – 0.3 T/IRM 1T.

Table T2. Hysteresis properties and estimated magnetic concentrations.

Core, section, interval (cm)	Depth (mbsf)	Depth (mcd)	M_r (μAm²/kg)	M_s (μAm²/kg)	H_c (mT)	M_r/M_s	Magnetite (%)
175-1075A-							
3H-5, 18-20	17.18	17.18	60.5	756	6.14	0.080	8.22E-04
3H-5, 58-60	17.58	17.58	39.9	824	4.47	0.048	8.96E-04
3H-6, 38-40	18.88	18.88	47	583	4.86	0.081	6.34E-04
4H-1, 118-120	21.68	22.94	101	703	9.51	0.144	7.64E-04
4H-2, 98-100	22.98	24.24	29.8	714	3.98	0.042	7.76E-04
4H-3, 138-140	24.88	26.14	99.4	957	8.91	0.104	1.04E-03
4H-4, 58-60	25.58	26.84	70.5	486	9.63	0.145	5.28E-04
15H-5, 38-40	129.91	143.12	456	5090	9.73	0.090	5.53E-03
15H-5, 118-120	130.71	143.92	88.6	1150	7.41	0.077	1.25E-03
15H-6, 58-60	131.61	144.82	73.2	760	10.4	0.096	8.26E-04
16H-3, 138-140	138.88	153.67	74.5	1030	6.08	0.072	1.12E-03

Note: M_r = saturation remanence, M_s = saturation magnetization, H_c = coercivity.

Table T3. XRF core-scanner results and shipboard susceptibility data interpolated to the XRF sampling positions. (Continued on next nine pages).

Core, section, top (cm)	Depth (mbsf)	Depth (mcd)	K (cps)	Ca (cps)	Ti (cps)	Mn (cps)	Fe (cps)	Susceptibility ($\times 10^{-6}$)
175-1075A-								
3H-3, 5	14.05	14.05	119	84	95	49	3664	531
3H-3, 10	14.10	14.10	104	69	90	36	2952	465
3H-3, 15	14.15	14.15	128	69	82	34	2972	465
3H-3, 20	14.20	14.20	107	70	77	29	2663	488
3H-3, 25	14.25	14.25	123	74	72	27	3129	491
3H-3, 30	14.30	14.30	104	69	86	8	2828	484
3H-3, 35	14.35	14.35	98	80	83	15	2687	476
3H-3, 40	14.40	14.40	91	89	87	0	2725	487
3H-3, 45	14.45	14.45	96	82	75	45	3110	498
3H-3, 50	14.50	14.50	110	83	79	39	3281	489
3H-3, 55	14.55	14.55	101	104	81	5	2632	479
3H-3, 60	14.60	14.60	108	120	90	14	2837	498
3H-3, 65	14.65	14.65	94	187	87	64	3149	533
3H-3, 70	14.70	14.70	113	231	86	11	2615	543
3H-3, 75	14.75	14.75	109	176	89	63	3627	542
3H-3, 80	14.80	14.80	109	198	78	8	2865	563
3H-3, 85	14.85	14.85	74	190	93	57	3160	572
3H-3, 90	14.90	14.90	118	197	95	49	2875	572
3H-3, 95	14.95	14.95	121	207	89	25	3095	571
3H-3, 100	15.00	15.00	109	209	88	43	2847	557
3H-3, 105	15.05	15.05	124	289	87	42	2879	544
3H-3, 110	15.10	15.10	114	248	78	56	3040	518
3H-3, 115	15.15	15.15	92	124	70	27	2383	519
3H-3, 120	15.20	15.20	101	228	75	20	2807	532
3H-3, 125	15.25	15.25	120	154	94	42	2924	549
3H-3, 130	15.30	15.30	121	128	90	44	2972	552
3H-3, 135	15.35	15.35	115	69	104	44	2959	552
3H-4, 5	15.55	15.55	109	92	95	53	2896	586
3H-4, 10	15.60	15.60	116	90	100	56	3382	641
3H-4, 15	15.65	15.65	110	84	104	46	3281	655
3H-4, 20	15.70	15.70	115	70	104	54	3302	673
3H-4, 25	15.75	15.75	142	76	106	46	3294	664
3H-4, 30	15.80	15.80	119	75	103	51	3357	633
3H-4, 35	15.85	15.85	71	120	59	13	3155	623
3H-4, 40	15.90	15.90	102	52	93	17	2852	602
3H-4, 45	15.95	15.95	95	48	72	65	4004	564
3H-4, 50	16.00	16.00	113	51	91	38	3217	540
3H-4, 55	16.05	16.05	110	49	93	44	3139	553
3H-4, 60	16.10	16.10	110	47	95	58	3141	543
3H-4, 65	16.15	16.15	116	50	100	15	2967	545
3H-4, 70	16.20	16.20	113	54	111	27	3012	547
3H-4, 75	16.25	16.25	117	62	109	18	3225	528
3H-4, 80	16.30	16.30	106	62	108	19	2911	512
3H-4, 85	16.35	16.35	136	61	109	62	3177	589
3H-4, 90	16.40	16.40	127	50	126	43	3382	605
3H-4, 95	16.45	16.45	124	57	95	51	3974	577
3H-4, 100	16.50	16.50	118	60	105	49	3557	520
3H-4, 105	16.55	16.55	117	60	102	47	3339	514
3H-4, 110	16.60	16.60	117	64	98	37	3280	563
3H-4, 115	16.65	16.65	105	42	95	54	3645	573
3H-4, 120	16.70	16.70	117	42	93	69	3780	564
3H-4, 125	16.75	16.75	123	43	104	44	3529	558
3H-4, 130	16.80	16.80	137	57	99	12	3402	530
3H-4, 135	16.85	16.85	140	53	122	64	3809	466
3H-5, 5	17.05	17.05	88	104	100	41	3197	369
3H-5, 10	17.10	17.10	84	82	78	44	3336	300
3H-5, 15	17.15	17.15	62	91	79	42	2967	296
3H-5, 20	17.20	17.20	102	97	80	10	3096	302
3H-5, 25	17.25	17.25	102	115	80	15	3077	318
3H-5, 30	17.30	17.30	95	96	84	47	2876	347
3H-5, 35	17.35	17.35	106	116	73	44	3291	362
3H-5, 40	17.40	17.40	70	57	92	16	3056	375
3H-5, 45	17.45	17.45	123	91	84	40	3163	402
3H-5, 50	17.50	17.50	130	78	112	9	2997	434
3H-5, 55	17.55	17.55	126	77	111	48	3302	480

Table T3 (continued).

Core, section, top (cm)	Depth (mbsf)	Depth (mcd)	K (cps)	Ca (cps)	Ti (cps)	Mn (cps)	Fe (cps)	Susceptibility ($\times 10^{-6}$)
3H-5, 60	17.60	17.60	132	55	98	42	2972	528
3H-5, 65	17.65	17.65	135	67	111	39	3388	551
3H-5, 70	17.70	17.70	144	78	118	31	3048	609
3H-5, 75	17.75	17.75	143	77	127	49	3484	656
3H-5, 80	17.80	17.80	156	64	118	21	3706	691
3H-5, 85	17.85	17.85	139	75	119	54	3818	712
3H-5, 90	17.90	17.90	158	86	123	46	3551	703
3H-5, 95	17.95	17.95	156	70	122	52	3742	726
3H-5, 100	18.00	18.00	144	85	119	53	3998	723
3H-5, 105	18.05	18.05	150	90	130	55	3988	712
3H-5, 110	18.10	18.10	140	74	118	66	3827	701
3H-5, 115	18.15	18.15	134	57	129	62	3875	700
3H-5, 120	18.20	18.20	131	57	109	59	3769	715
3H-5, 125	18.25	18.25	130	60	127	71	4145	743
3H-5, 130	18.30	18.30	140	58	130	56	3861	723
3H-5, 135	18.35	18.35	135	58	129	47	4005	710
3H-6, 5	18.55	18.55	95	107	97	48	3196	776
3H-6, 10	18.60	18.60	127	131	116	63	4010	835
3H-6, 15	18.65	18.65	140	172	115	83	4382	816
3H-6, 20	18.70	18.70	134	118	112	79	4426	779
3H-6, 25	18.75	18.75	148	169	122	76	3977	710
3H-6, 30	18.80	18.80	144	333	112	53	4052	682
3H-6, 35	18.85	18.85	133	242	90	34	3219	635
3H-6, 40	18.90	18.90	153	626	92	50	3096	600
3H-6, 45	18.95	18.95	141	419	92	64	3546	596
3H-6, 50	19.00	19.00	139	684	83	41	3068	574
3H-6, 55	19.05	19.05	134	465	87	22	3248	571
3H-6, 60	19.10	19.10	141	615	88	51	3004	530
3H-6, 65	19.15	19.15	139	651	83	53	3261	503
3H-6, 70	19.20	19.20	134	693	82	50	3030	489
3H-6, 75	19.25	19.25	143	707	85	22	2807	488
3H-6, 80	19.30	19.30	142	703	81	49	2967	483
3H-6, 85	19.35	19.35	114	497	73	50	2769	446
3H-6, 90	19.40	19.40	127	569	83	38	2733	411
3H-6, 95	19.45	19.45	125	516	77	35	2476	380
3H-6, 100	19.50	19.50	124	401	87	15	2545	372
3H-6, 105	19.55	19.55	62	252	50	4	1856	373
3H-6, 110	19.60	19.60	133	284	90	42	2834	393
3H-6, 115	19.65	19.65	120	258	82	45	2879	419
3H-6, 120	19.70	19.70	118	240	78	42	3080	427
3H-6, 125	19.75	19.75	89	171	80	48	2799	433
3H-6, 130	19.80	19.80	112	223	75	34	2989	423
3H-6, 135	19.85	19.85	120	265	82	22	2936	390
3H-6, 140	19.90	19.90	100	157	68	40	2680	406
3H-7, 5	20.05	20.05	106	135	90	46	2945	442
3H-7, 10	20.10	20.10	105	137	86	53	3061	493
3H-7, 15	20.15	20.15	123	181	82	52	2982	484
3H-7, 20	20.20	20.20	125	162	100	40	2814	453
3H-7, 25	20.25	20.25	122	141	96	13	2552	443
3H-7, 30	20.30	20.30	117	162	87	53	2687	441
3H-7, 35	20.35	20.35	116	176	94	15	2713	452
3H-7, 40	20.40	20.40	110	140	93	19	2631	445
3H-7, 45	20.45	20.45	124	143	87	22	2627	432
3H-7, 50	20.50	20.50	108	160	96	25	2585	447
3H-7, 55	20.55	20.55	111	140	76	45	2427	459
3H-7, 60	20.60	20.60	124	155	87	18	2508	467
3H-7, 65	20.65	20.65	108	124	81	40	2559	462
3H-7, 70	20.70	20.70	98	131	78	37	2529	499
4H-1, 30	20.80	22.06	92	287	64	18	2430	510
4H-1, 35	20.85	22.11	93	385	53	20	2474	494
4H-1, 40	20.90	22.16	90	457	49	31	2360	487
4H-1, 45	20.95	22.21	93	701	68	27	2105	478
4H-1, 50	21.00	22.26	111	883	54	14	2145	467
4H-1, 55	21.05	22.31	106	832	63	36	2281	447
4H-1, 60	21.10	22.36	118	782	62	24	2411	468
4H-1, 65	21.15	22.41	130	861	86	36	2119	484
4H-1, 70	21.20	22.46	105	645	72	14	1871	476
4H-1, 75	21.25	22.51	121	509	79	33	2525	489
4H-1, 80	21.30	22.56	116	269	74	22	2691	499

Table T3 (continued).

Core, section, top (cm)	Depth (mbsf)	Depth (mcd)	K (cps)	Ca (cps)	Ti (cps)	Mn (cps)	Fe (cps)	Susceptibility ($\times 10^{-6}$)
4H-1, 85	21.35	22.61	107	309	76	18	2409	485
4H-1, 90	21.40	22.66	103	403	62	36	2472	452
4H-1, 95	21.45	22.71	114	552	70	16	2302	427
4H-1, 100	21.50	22.76	91	353	63	35	2402	404
4H-1, 105	21.55	22.81	96	293	67	37	2695	387
4H-1, 110	21.60	22.86	80	195	66	45	2432	373
4H-1, 115	21.65	22.91	93	191	69	33	2445	380
4H-1, 120	21.70	22.96	90	119	82	5	2842	374
4H-1, 125	21.75	23.01	85	122	85	33	2519	339
4H-1, 130	21.80	23.06	87	112	87	15	2398	321
4H-1, 135	21.85	23.11	58	150	71	29	2077	335
4H-2, 5	22.05	23.31	109	134	82	43	2608	386
4H-2, 10	22.10	23.36	104	97	79	19	2491	415
4H-2, 15	22.15	23.41	99	112	75	42	2636	429
4H-2, 20	22.20	23.46	90	115	81	37	2702	421
4H-2, 25	22.25	23.51	102	113	81	33	2696	391
4H-2, 30	22.30	23.56	100	89	83	15	2476	418
4H-2, 35	22.35	23.61	100	81	88	15	2524	425
4H-2, 40	22.40	23.66	104	72	84	31	2542	417
4H-2, 45	22.45	23.71	108	75	82	38	2743	380
4H-2, 50	22.50	23.76	79	56	75	13	2502	362
4H-2, 60	22.60	23.86	66	92	74	47	2993	382
4H-2, 65	22.65	23.91	108	128	96	53	3079	420
4H-2, 70	22.70	23.96	102	126	75	14	2618	432
4H-2, 75	22.75	24.01	100	105	86	29	2821	450
4H-2, 80	22.80	24.06	118	105	104	37	2801	451
4H-2, 85	22.85	24.11	103	63	86	52	3362	492
4H-2, 90	22.90	24.16	119	97	101	55	2892	529
4H-2, 95	22.95	24.21	108	68	98	20	2860	514
4H-2, 100	23.00	24.26	126	93	101	65	3019	485
4H-2, 105	23.05	24.31	120	97	102	58	2694	437
4H-2, 110	23.10	24.36	109	79	97	49	2778	450
4H-2, 115	23.15	24.41	111	87	97	59	3073	479
4H-2, 120	23.20	24.46	70	75	94	40	2603	482
4H-2, 125	23.25	24.51	102	107	89	59	2844	451
4H-2, 130	23.30	24.56	118	145	98	16	2559	449
4H-2, 135	23.35	24.61	105	152	89	53	3172	486
4H-3, 5	23.55	24.81	138	181	100	51	3269	505
4H-3, 10	23.60	24.86	124	156	96	43	2944	539
4H-3, 15	23.65	24.91	81	152	85	44	3077	532
4H-3, 20	23.70	24.96	118	221	102	42	2904	522
4H-3, 25	23.75	25.01	107	239	91	15	2708	505
4H-3, 30	23.80	25.06	109	219	82	41	2838	482
4H-3, 35	23.85	25.11	102	224	72	39	2737	467
4H-3, 40	23.90	25.16	113	263	76	32	3024	510
4H-3, 45	23.95	25.21	116	302	73	26	2709	506
4H-3, 50	24.00	25.26	112	409	75	13	2812	464
4H-3, 55	24.05	25.31	111	233	80	33	2392	455
4H-3, 60	24.10	25.36	109	127	92	44	2863	466
4H-3, 65	24.15	25.41	125	80	91	49	2866	462
4H-3, 70	24.20	25.46	111	73	108	14	2744	438
4H-3, 75	24.25	25.51	86	45	91	46	2614	457
4H-3, 80	24.30	25.56	107	58	98	10	2572	458
4H-3, 85	24.35	25.61	119	48	92	45	2781	441
4H-3, 90	24.40	25.66	114	67	102	39	2613	407
4H-3, 95	24.45	25.71	81	54	91	47	2816	363
4H-3, 100	24.50	25.76	104	118	85	9	2237	337
4H-3, 105	24.55	25.81	110	80	89	20	2483	359
4H-3, 110	24.60	25.86	114	79	83	38	2480	348
4H-3, 115	24.65	25.91	101	84	98	36	2459	338
4H-3, 120	24.70	25.96	94	55	82	14	2429	309
4H-3, 125	24.75	26.01	99	54	79	44	2423	302
4H-3, 130	24.80	26.06	77	44	91	21	2369	284
4H-3, 135	24.85	26.11	95	57	84	12	2429	317
4H-4, 5	25.05	26.31	99	37	88	40	3035	429
4H-4, 10	25.10	26.36	115	44	92	46	3053	488
4H-4, 15	25.15	26.41	110	44	87	35	2463	488
4H-4, 20	25.20	26.46	123	61	95	29	2464	488
4H-4, 25	25.25	26.51	110	75	81	41	2750	478

Table T3 (continued).

Core, section, top (cm)	Depth (mbsf)	Depth (mcd)	K (cps)	Ca (cps)	Ti (cps)	Mn (cps)	Fe (cps)	Susceptibility ($\times 10^{-6}$)
4H-4, 30	25.30	26.56	94	36	91	57	2851	481
4H-4, 35	25.35	26.61	111	42	98	13	2571	479
4H-4, 40	25.40	26.66	124	104	91	27	2232	488
4H-4, 45	25.45	26.71	108	52	85	41	2948	474
4H-4, 50	25.50	26.76	120	49	91	18	2897	465
4H-4, 55	25.55	26.81	107	48	88	15	2725	475
4H-4, 60	25.60	26.86	97	43	86	20	2550	516
4H-4, 65	25.65	26.91	113	87	97	22	3295	569
4H-4, 70	25.70	26.96	108	36	89	45	3114	566
4H-4, 75	25.75	27.01	114	37	98	53	2868	543
4H-4, 80	25.8	27.06	113	36	112	53	2930	513
4H-4, 85	25.850	27.11	106	60	111	38	3034	519
4H-4, 90	25.90	27.16	114	64	113	30	2962	557
4H-4, 95	25.95	27.21	120	60	108	52	3158	610
4H-4, 100	26.00	27.26	116	55	108	45	2920	648
4H-4, 105	26.05	27.31	127	83	98	53	3134	683
4H-4, 110	26.10	27.36	133	83	123	20	3085	688
4H-4, 115	26.15	27.41	122	60	98	48	3266	720
4H-4, 120	26.20	27.46	127	73	108	13	3141	732
4H-4, 125	26.25	27.51	127	98	106	12	3018	696
4H-4, 130	26.30	27.56	135	76	101	22	3135	658
4H-4, 135	26.35	27.61	127	75	94	45	3115	631
4H-5, 5	26.55	27.81	129	47	110	53	3636	672
4H-5, 10	26.60	27.86	131	67	99	43	3252	667
4H-5, 15	26.65	27.91	111	70	90	42	3104	609
4H-5, 20	26.70	27.96	120	74	115	13	3371	625
4H-5, 25	26.75	28.01	132	63	116	51	3326	646
4H-5, 30	26.80	28.06	116	57	103	49	3798	636
4H-5, 35	26.85	28.11	105	47	114	47	3625	640
4H-5, 40	26.90	28.16	137	48	110	61	3632	706
4H-5, 45	26.95	28.21	139	44	143	56	3759	791
4H-5, 50	27.00	28.26	161	51	130	52	3605	797
4H-5, 55	27.05	28.31	154	48	141	12	3497	830
4H-5, 60	27.10	28.36	139	38	136	42	3748	860
4H-5, 65	27.15	28.41	152	57	136	27	3840	864
4H-5, 70	27.20	28.46	157	48	131	68	3853	874
4H-5, 75	27.25	28.51	149	65	116	50	3619	889
4H-5, 80	27.30	28.56	133	42	108	53	3607	871
4H-5, 85	27.35	28.61	134	31	121	64	3509	838
4H-5, 90	27.40	28.66	135	31	117	32	3573	814
4H-5, 95	27.45	28.71	128	36	124	28	3700	810
4H-5, 100	27.50	28.76	138	39	117	27	3623	817
4H-5, 105	27.55	28.81	130	38	113	34	3582	814
4H-5, 110	27.60	28.86	114	29	110	53	3778	768
4H-5, 115	27.65	28.91	136	36	103	61	3639	725
4H-5, 120	27.70	28.96	126	37	110	43	3351	713
4H-5, 125	27.75	29.01	132	38	107	58	3715	720
4H-5, 130	27.80	29.06	135	44	117	49	3585	726
4H-5, 135	27.85	29.11	134	51	116	66	3482	706
4H-6, 5	28.05	29.31	126	108	105	66	3739	700
4H-6, 10	28.10	29.36	129	144	112	20	3123	749
4H-6, 15	28.15	29.41	136	122	107	21	3456	767
4H-6, 20	28.20	29.46	121	169	101	66	3368	722
4H-6, 25	28.25	29.51	129	167	104	24	3587	693
4H-6, 30	28.30	29.56	122	159	94	60	3066	652
4H-6, 35	28.35	29.61	126	138	118	47	3267	647
4H-6, 40	28.40	29.66	134	160	120	56	3164	639
4H-6, 45	28.45	29.71	118	87	80	60	3667	654
4H-6, 50	28.50	29.76	133	175	111	66	3826	681
4H-6, 55	28.55	29.81	127	105	102	12	3284	642
4H-6, 60	28.60	29.86	128	106	99	62	3796	556
4H-6, 65	28.65	29.91	115	62	89	18	3211	522
4H-6, 70	28.70	29.96	131	128	90	38	3043	519
4H-6, 75	28.75	30.01	118	116	85	17	3443	566
4H-6, 80	28.8	30.06	123	95	93	42	3626	614
4H-6, 85	28.85	30.11	138	78	96	57	3763	626
4H-6, 90	28.90	30.16	137	126	101	60	3304	614
4H-6, 95	28.95	30.21	139	161	121	14	3038	591
4H-6, 100	29.00	30.26	153	169	112	42	2836	587

Table T3 (continued).

Core, section, top (cm)	Depth (mbsf)	Depth (mcd)	K (cps)	Ca (cps)	Ti (cps)	Mn (cps)	Fe (cps)	Susceptibility ($\times 10^{-6}$)
4H-6, 105	29.05	30.31	140	133	116	43	3014	599
4H-6, 110	29.10	30.36	135	81	100	40	3082	598
4H-6, 115	29.15	30.41	136	67	118	50	3166	572
4H-6, 120	29.20	30.46	133	64	113	6	3385	519
4H-6, 125	29.25	30.51	91	54	81	30	2301	473
4H-6, 130	29.30	30.56	123	74	94	30	2834	449
4H-6, 135	29.35	30.61	126	64	98	54	3619	421
4H-7, 5	29.55	30.81	109	31	84	25	3214	452
4H-7, 10	29.60	30.86	127	40	101	0	3252	546
4H-7, 15	29.65	30.91	147	55	133	58	3775	549
4H-7, 20	29.70	30.96	136	36	120	42	3427	582
4H-7, 25	29.75	31.01	146	46	124	16	3456	617
4H-7, 30	29.80	31.06	135	44	126	24	3515	623
4H-7, 35	29.85	31.11	127	42	115	54	3660	671
4H-7, 40	29.90	31.16	135	41	118	51	3767	718
4H-7, 45	29.95	31.21	132	35	121	67	3892	754
4H-7, 50	30.00	31.26	123	39	126	46	3797	763
4H-7, 55	30.05	31.31	136	31	109	52	3591	608
5H-1, 5	30.05	31.36	106	616	66	8	2299	539
5H-1, 10	30.10	31.41	111	525	67	13	2425	511
5H-1, 15	30.15	31.46	102	440	68	31	2420	486
5H-1, 20	30.20	31.51	95	400	73	30	2672	491
5H-1, 25	30.25	31.56	93	150	69	18	2438	402
5H-1, 30	30.30	31.61	67	179	85	27	2442	358
5H-1, 35	30.35	31.66	62	84	73	30	2263	424
5H-1, 40	30.40	31.71	102	103	72	32	2489	403
5H-1, 45	30.45	31.76	60	91	69	17	2289	336
5H-1, 50	30.50	31.81	77	114	61	39	2284	300
5H-1, 55	30.55	31.86	49	97	64	18	2216	313
5H-1, 60	30.60	31.91	73	105	66	17	2199	329
5H-1, 65	30.65	31.96	66	82	63	30	2007	315
5H-1, 70	30.70	32.01	52	95	59	17	2280	305
5H-1, 75	30.75	32.06	85	120	59	13	2343	339
5H-1, 80	30.80	32.11	87	170	73	11	2559	386
5H-1, 85	30.85	32.16	87	206	81	45	2527	404
5H-1, 90	30.90	32.21	61	160	81	10	2271	414
5H-1, 95	30.95	32.26	82	171	70	16	2227	406
5H-1, 100	31.00	32.31	79	154	76	13	2461	407
5H-1, 105	31.05	32.36	94	180	76	46	2506	371
5H-1, 110	31.10	32.41	99	183	75	14	2338	342
5H-1, 115	31.15	32.46	105	175	75	39	2422	370
5H-1, 120	31.20	32.51	100	154	72	11	2366	354
5H-1, 125	31.25	32.56	110	156	73	5	2387	338
5H-1, 130	31.30	32.61	103	139	74	16	2435	345
5H-1, 135	31.35	32.66	97	112	77	12	2364	
15H-4, 5	128.23	141.44	74	20	56	29	1823	450
15H-4, 10	128.28	141.49	77	26	61	30	1895	452
15H-4, 15	128.33	141.54	107	36	92	35	2414	488
15H-4, 20	128.38	141.59	110	30	97	36	2647	513
15H-4, 25	128.43	141.64	93	26	70	36	2226	472
15H-4, 30	128.48	141.69	109	30	83	58	2835	512
15H-4, 35	128.53	141.74	113	37	84	14	2731	462
15H-4, 40	128.58	141.79	117	31	105	15	2722	384
15H-4, 45	128.63	141.84	105	30	89	44	2548	318
15H-4, 49	128.67	141.88	137	47	110	17	2922	374
15H-4, 56	128.74	141.95	45	18	52	0	1329	487
15H-4, 60	128.78	141.99	94	26	89	54	2859	484
15H-4, 65	128.83	142.04	99	30	82	11	2677	441
15H-4, 70	128.88	142.09	102	38	76	48	3103	370
15H-4, 75	128.93	142.14	91	29	78	27	2340	349
15H-4, 80	128.98	142.19	104	33	81	45	2740	323
15H-4, 85	129.03	142.24	57	21	50	24	1644	345
15H-4, 90	129.08	142.29	98	34	79	50	2849	341
15H-4, 95	129.13	142.34	88	32	66	48	2273	330
15H-4, 100	129.18	142.39	100	35	83	25	2555	335
15H-4, 105	129.23	142.44	93	35	61	47	2470	302
15H-4, 110	129.28	142.49	72	28	51	28	2305	282
15H-4, 115	129.33	142.54	79	32	59	58	2696	250
15H-4, 120	129.38	142.59	80	32	57	46	2364	240

Table T3 (continued).

Core, section, top (cm)	Depth (mbsf)	Depth (mcd)	K (cps)	Ca (cps)	Ti (cps)	Mn (cps)	Fe (cps)	Susceptibility ($\times 10^{-6}$)
15H-4, 125	129.43	142.64	82	30	59	51	2492	297
15H-4, 130	129.48	142.69	103	33	65	47	3177	342
15H-5, 5	129.53	142.74	101	41	78	47	2597	397
15H-5, 10	129.58	142.79	95	31	82	44	2886	415
15H-5, 15	129.63	142.84	97	33	79	29	2310	320
15H-5, 20	129.68	142.89	87	27	61	46	2315	227
15H-5, 25	129.73	142.94	59	21	57	25	2266	216
15H-5, 32	129.80	143.01	73	28	58	8	2245	227
15H-5, 35	129.83	143.04	78	30	59	13	2420	247
15H-5, 40	129.88	143.09	88	36	65	11	2432	260
15H-5, 45	129.93	143.14	83	26	55	21	2592	263
15H-5, 50	129.98	143.19	106	30	74	33	2938	289
15H-5, 55	130.03	143.24	75	27	63	11	2532	255
15H-5, 60	130.08	143.29	73	20	59	30	2442	236
15H-5, 65	130.13	143.34	67	24	55	25	2054	269
15H-5, 70	130.18	143.39	90	26	62	36	2602	291
15H-5, 73	130.21	143.42	98	33	67	22	2605	314
15H-5, 78	130.26	143.47	59	19	46	22	1922	363
15H-5, 85	130.33	143.54	108	32	85	42	2814	402
15H-5, 90	130.38	143.59	85	28	63	16	2268	442
15H-5, 95	130.43	143.64	126	28	92	37	3051	434
15H-5, 100	130.48	143.69	86	27	58	28	2461	422
15H-5, 105	130.53	143.74	122	31	88	55	3186	419
15H-5, 110	130.58	143.79	121	30	75	46	3332	432
15H-5, 115	130.63	143.84	98	29	68	17	2467	472
15H-5, 120	130.68	143.89	115	22	93	45	3009	488
15H-5, 125	130.73	143.94	126	35	98	14	3163	500
15H-5, 130	130.78	143.99	125	35	101	42	2699	525
15H-5, 135	130.83	144.04	113	32	80	48	2596	542
15H-5, 140	130.88	144.09	88	17	70	56	3136	535
15H-5, 145	130.93	144.14	111	28	70	47	2972	545
15H-6, 10	131.08	144.29	189	58	125	22	3614	644
15H-6, 15	131.13	144.34	120	60	87	44	2648	669
15H-6, 20	131.18	144.39	109	40	77	48	2829	667
15H-6, 25	131.23	144.44	137	60	104	18	3279	647
15H-6, 30	131.28	144.49	141	70	106	27	2993	629
15H-6, 35	131.33	144.54	80	167	80	12	2596	618
15H-6, 40	131.38	144.59	140	151	88	57	3286	610
15H-6, 45	131.43	144.64	144	189	92	54	3115	571
15H-6, 50	131.48	144.69	142	192	98	52	3034	537
15H-6, 55	131.53	144.74	123	145	80	45	2795	489
15H-6, 60	131.58	144.79	115	103	83	42	2754	474
15H-6, 65	131.63	144.84	149	88	93	16	2894	474
15H-6, 70	131.68	144.89	64	177	67	38	2380	476
15H-6, 75	131.73	144.94	112	94	75	42	2523	487
15H-6, 80	131.78	144.99	112	67	80	49	2447	498
15H-6, 85	131.83	145.04	118	42	87	9	2908	489
15H-6, 90	131.88	145.09	133	55	98	60	3330	438
15H-6, 95	131.93	145.14	116	42	83	59	3107	427
15H-6, 100	131.98	145.19	112	50	85	59	2848	422
15H-6, 105	132.03	145.24	107	36	73	37	2834	415
15H-6, 110	132.08	145.29	116	47	108	58	2953	386
15H-6, 115	132.13	145.34	105	56	80	38	2520	370
15H-6, 120	132.18	145.39	99	47	82	46	3359	388
15H-6, 125	132.23	145.44	73	28	58	36	2174	388
15H-6, 130	132.28	145.49	113	44	85	30	2685	373
15H-6, 135	132.33	145.54	82	46	63	22	2366	363
15H-6, 140	132.38	145.59	85	32	62	19	2186	397
15H-6, 145	132.43	145.64	135	35	79	10	2503	392
15H-7, 5	132.53	145.74	145	45	97	57	3540	398
15H-7, 10	132.58	145.79	84	39	77	34	2262	366
15H-7, 15	132.63	145.84	66	31	52	42	2622	354
15H-7, 20	132.68	145.89	79	31	73	44	2726	389
15H-7, 25	132.73	145.94	75	26	63	35	2540	421
15H-7, 35	132.83	146.04	98	23	82	42	2710	551
15H-7, 40	132.88	146.09	131	53	86	40	3054	435
15H-7, 45	132.93	146.14	85	32	68	15	2722	377
15H-7, 50	132.98	146.19	75	21	70	62	2666	374
15H-7, 55	133.03	146.24	75	24	58	9	2800	385

Table T3 (continued).

Core, section, top (cm)	Depth (mbsf)	Depth (mcd)	K (cps)	Ca (cps)	Ti (cps)	Mn (cps)	Fe (cps)	Susceptibility ($\times 10^{-6}$)
15H-7, 60	133.08	146.29	92	40	75	57	2816	417
15H-7, 65	133.13	146.34	99	34	70	14	2772	523
15H-7, 70	133.18	146.39	113	40	88	48	3180	561
15H-7, 75	133.23	146.44	127	33	103	50	3184	526
15H-7, 80	133.28	146.49	119	48	72	39	2894	477
15H-7, 85	133.33	146.54	99	34	72	16	2342	403
15H-7, 90	133.38	146.59	97	34	61	41	2613	318
15H-7, 95	133.43	146.64	83	31	63	18	2800	275
15H-7, 100	133.48	146.69	63	27	54	27	2275	270
15H-7, 105	133.53	146.74	77	33	57	42	2563	274
15H-7, 120	133.68	146.89	72	23	62	14	2395	286
15H-7, 125	133.73	146.94	75	28	55	14	2237	266
15H-7, 130	133.78	146.99	76	29	54	15	2255	267
15H-7, 145	133.93	147.14	93	36	68	35	2269	388
15H-8, 5	134.03	147.24	149	34	100	49	3381	353
15H-8, 10	134.08	147.29	133	35	96	49	3344	354
15H-8, 15	134.13	147.34	139	38	89	41	3155	341
15H-8, 20	134.18	147.39	136	31	91	34	3185	313
15H-8, 25	134.23	147.44	103	33	80	7	2482	319
15H-8, 30	134.28	147.49	99	28	66	35	2737	327
15H-8, 35	134.33	147.54	133	25	84	57	3188	390
15H-8, 40	134.38	147.59	112	29	85	66	2907	427
15H-8, 45	134.43	147.64	136	30	92	45	3309	445
15H-8, 50	134.48	147.69	126	26	95	18	2808	444
15H-8, 55	134.53	147.74	128	27	78	58	3296	453
15H-8, 60	134.58	147.79	138	30	100	17	2879	486
15H-8, 65	134.63	147.84	164	32	108	15	3003	522
15H-8, 70	134.68	147.89	162	25	109	62	3416	553
15H-8, 75	134.73	147.94	171	24	107	46	3332	550
15H-8, 85	134.83	148.04	179	34	99	60	3776	666
16H-1, 5	134.55	149.34	166	32	143	29	3951	688
16H-1, 10	134.60	149.39	110	37	87	38	3171	651
16H-1, 15	134.65	149.44	153	31	113	61	3656	677
16H-1, 20	134.70	149.49	135	34	112	16	3302	636
16H-1, 25	134.75	149.54	160	35	114	72	3919	613
16H-1, 35	134.85	149.64	145	33	102	72	4605	594
16H-1, 40	134.90	149.69	145	40	117	30	3660	627
16H-1, 45	134.95	149.74	153	63	124	53	3810	637
16H-1, 50	135.00	149.79	171	191	132	67	4019	680
16H-1, 55	135.05	149.84	131	182	103	55	3030	628
16H-1, 60	135.10	149.89	133	169	106	29	3076	563
16H-1, 65	135.15	149.94	112	81	96	59	3148	419
16H-1, 85	135.35	150.14	99	56	99	49	3496	384
16H-1, 95	135.45	150.24	108	49	79	70	3732	523
16H-1, 100	135.50	150.29	96	48	83	70	3663	600
16H-1, 105	135.55	150.34	93	43	82	60	3072	649
16H-1, 110	135.60	150.39	85	37	65	21	3238	710
16H-1, 115	135.65	150.44	123	37	82	76	4254	769
16H-1, 120	135.70	150.49	143	48	106	62	4240	743
16H-1, 125	135.75	150.54	151	52	122	77	4161	727
16H-1, 130	135.80	150.59	141	46	116	53	3806	707
16H-1, 135	135.85	150.64	143	39	119	67	3988	739
16H-1, 140	135.90	150.69	99	30	79	30	2241	770
16H-1, 145	135.95	150.74	194	46	152	68	3907	658
16H-2, 5	136.05	150.84	150	60	117	46	3752	531
16H-2, 10	136.10	150.89	160	48	104	67	4083	453
16H-2, 15	136.15	150.94	166	44	114	27	3827	449
16H-2, 20	136.20	150.99	111	38	75	36	2855	437
16H-2, 25	136.25	151.04	123	49	81	45	3271	459
16H-2, 30	136.30	151.09	170	48	111	57	3695	477
16H-2, 35	136.35	151.14	164	48	104	57	3584	448
16H-2, 40	136.40	151.19	152	42	100	65	3266	421
16H-2, 45	136.45	151.24	139	41	80	46	2999	428
16H-2, 55	136.55	151.34	161	38	109	65	3193	457
16H-2, 60	136.60	151.39	130	36	97	61	3338	519
16H-2, 65	136.65	151.44	141	37	102	43	3298	514
16H-2, 70	136.70	151.49	125	40	90	38	3015	528
16H-2, 75	136.75	151.54	144	43	90	50	3036	555
16H-2, 80	136.80	151.59	171	74	115	70	3726	578

Table T3 (continued).

Core, section, top (cm)	Depth (mbsf)	Depth (mcd)	K (cps)	Ca (cps)	Ti (cps)	Mn (cps)	Fe (cps)	Susceptibility ($\times 10^{-6}$)
16H-2, 85	136.85	151.64	109	47	71	15	2173	672
16H-2, 90	136.90	151.69	192	70	117	35	3721	740
16H-2, 95	136.95	151.74	164	31	111	71	3649	746
16H-2, 100	137.00	151.79	185	33	130	61	3914	753
16H-2, 105	137.05	151.84	193	43	132	19	3468	749
16H-2, 110	137.10	151.89	176	32	123	36	3730	754
16H-2, 115	137.15	151.94	147	33	116	42	3203	742
16H-2, 120	137.20	151.99	182	36	131	55	3663	710
16H-2, 125	137.25	152.04	167	33	116	65	3684	701
16H-2, 130	137.30	152.09	175	33	119	46	3617	692
16H-2, 135	137.35	152.14	172	35	112	61	3670	694
16H-2, 140	137.40	152.19	172	34	108	61	3992	676
16H-2, 145	137.45	152.24	180	31	118	52	4022	745
16H-3, 5	137.55	152.34	188	47	123	68	4165	843
16H-3, 10	137.60	152.39	176	34	126	49	4205	938
16H-3, 15	137.65	152.44	199	41	154	80	4889	948
16H-3, 20	137.70	152.49	166	38	121	59	4185	925
16H-3, 25	137.75	152.54	177	36	124	58	3656	833
16H-3, 30	137.80	152.59	174	33	115	67	3686	777
16H-3, 35	137.85	152.64	182	40	141	52	4252	769
16H-3, 40	137.90	152.69	114	29	88	51	2951	768
16H-3, 45	137.95	152.74	127	18	99	15	3286	755
16H-3, 50	138.00	152.79	119	31	93	40	2706	742
16H-3, 55	138.05	152.84	144	29	116	60	3479	736
16H-3, 60	138.10	152.89	96	24	82	43	2628	753
16H-3, 65	138.15	152.94	106	22	92	14	2838	764
16H-3, 70	138.20	152.99	134	31	120	45	3356	741
16H-3, 75	138.25	153.04	160	37	123	57	3407	731
16H-3, 80	138.30	153.09	124	28	112	46	3123	717
16H-3, 85	138.35	153.14	140	42	107	22	3353	723
16H-3, 90	138.40	153.19	120	40	103	55	3101	730
16H-3, 95	138.45	153.24	148	52	124	62	3431	688
16H-3, 100	138.50	153.29	144	43	126	72	3716	653
16H-3, 105	138.55	153.34	125	29	113	42	3253	610
16H-3, 110	138.60	153.39	144	35	107	30	3519	596
16H-3, 115	138.65	153.44	153	39	124	65	3900	590
16H-3, 120	138.70	153.49	145	32	114	55	3482	605
16H-3, 125	138.75	153.54	112	38	87	22	3784	580
16H-3, 130	138.80	153.59	118	39	103	52	3704	512
16H-3, 135	138.85	153.64	134	46	112	67	3607	504
16H-3, 140	138.90	153.69	115	50	81	15	3005	481
16H-3, 145	138.95	153.74	130	52	95	55	3278	456
16H-4, 5	139.05	153.84	130	38	91	41	3744	443
16H-4, 10	139.10	153.89	65	22	64	44	2758	417
16H-4, 15	139.15	153.94	108	39	88	11	3074	389
16H-4, 20	139.20	153.99	86	32	64	37	2830	408
16H-4, 25	139.25	154.04	72	32	62	17	2498	461
16H-4, 30	139.30	154.09	92	40	82	44	2805	477
16H-4, 35	139.35	154.14	102	37	81	49	2701	444
16H-4, 40	139.40	154.19	97	37	86	50	3177	410
16H-4, 45	139.45	154.24	104	38	82	39	3005	396
16H-4, 50	139.50	154.29	81	32	70	16	2855	429
16H-4, 55	139.55	154.34	77	29	80	40	2759	423
16H-4, 60	139.60	154.39	94	32	72	47	3034	400
16H-4, 65	139.65	154.44	106	32	84	52	2648	397
16H-4, 70	139.70	154.49	83	31	72	29	2803	410
16H-4, 75	139.75	154.54	100	25	78	37	3007	390
16H-4, 80	139.80	154.59	71	24	57	28	2476	377
16H-4, 85	139.85	154.64	86	31	63	21	2457	377
16H-4, 90	139.90	154.69	99	26	81	56	2984	387
16H-4, 95	139.95	154.74	95	24	73	12	2779	385
16H-4, 100	140.00	154.79	108	32	79	55	3025	382
16H-4, 105	140.05	154.84	87	16	64	43	2900	395
16H-4, 110	140.10	154.89	107	30	80	51	3062	420
16H-4, 115	140.15	154.94	103	33	87	48	2872	420
16H-4, 120	140.20	154.99	91	24	66	44	2835	407
16H-4, 125	140.25	155.04	78	30	71	12	2786	400
16H-4, 130	140.30	155.09	73	25	58	35	2297	404
16H-4, 135	140.35	155.14	108	25	81	32	2805	420

Table T3 (continued).

Core, section, top (cm)	Depth (mbsf)	Depth (mcd)	K (cps)	Ca (cps)	Ti (cps)	Mn (cps)	Fe (cps)	Susceptibility ($\times 10^{-6}$)
16H-4, 140	140.4	155.19	103	35	90	41	2939	431
16H-4, 145	140.45	155.24	94	24	68	31	2496	427
16H-5, 5	140.55	155.34	149	33	102	34	3058	462
16H-5, 10	140.6	155.39	116	24	86	43	2999	494
16H-5, 15	140.65	155.44	90	28	60	37	2382	488
16H-5, 20	140.70	155.49	147	39	106	49	3027	480
16H-5, 25	140.75	155.54	119	33	89	24	2900	491
16H-5, 30	140.80	155.59	99	33	79	44	3305	485
16H-5, 35	140.85	155.64	117	46	92	15	3000	467
16H-5, 40	140.90	155.69	138	54	101	58	2903	462
16H-5, 45	140.95	155.74	124	63	102	55	3052	457
16H-5, 50	141.00	155.79	126	74	96	64	2801	454
16H-5, 55	141.05	155.84	119	65	90	31	2790	439
16H-5, 60	141.10	155.89	118	48	93	36	3068	425
16H-5, 65	141.15	155.94	91	27	68	24	2581	432
16H-5, 70	141.20	155.99	122	45	91	12	2347	442
16H-5, 75	141.25	156.04	104	30	90	50	3119	444
16H-5, 80	141.30	156.09	106	39	95	53	2939	460
16H-5, 85	141.35	156.14	107	50	77	52	2739	460
16H-5, 90	141.40	156.19	110	50	83	46	2711	460
16H-5, 95	141.45	156.24	143	55	104	18	2933	478
16H-5, 100	141.50	156.29	136	48	92	41	3180	468
16H-5, 105	141.55	156.34	119	50	92	45	2786	494
16H-5, 110	141.60	156.39	137	42	98	28	2935	532
16H-5, 115	141.65	156.44	110	50	110	59	3186	515
16H-5, 120	141.70	156.49	138	95	114	57	3247	508
16H-5, 125	141.75	156.54	144	136	113	41	2963	502
16H-5, 130	141.80	156.59	148	158	118	29	2887	488
16H-5, 135	141.85	156.64	122	135	121	51	3122	490
16H-5, 140	141.90	156.69	115	87	103	41	2787	489
16H-5, 145	141.95	156.74	158	170	125	58	3177	490
16H-6, 5	142.05	156.84	159	108	131	65	3628	518
16H-6, 10	142.10	156.89	131	91	107	55	3315	525
16H-6, 15	142.15	156.94	115	243	101	47	2798	563
16H-6, 20	142.20	156.99	133	340	115	61	2952	586
16H-6, 25	142.25	157.04	120	280	136	45	2786	558
16H-6, 30	142.30	157.09	136	118	113	56	3617	520
16H-6, 35	142.35	157.14	77	80	63	15	2322	462
16H-6, 40	142.40	157.19	108	64	87	31	2909	416
16H-6, 45	142.45	157.24	76	35	66	48	2868	418
16H-6, 50	142.50	157.29	83	65	77	40	2775	449
16H-6, 55	142.55	157.34	101	73	79	50	2947	486
16H-6, 60	142.60	157.39	93	108	67	46	2904	527
16H-6, 65	142.65	157.44	98	124	81	50	3211	579
16H-6, 70	142.70	157.49	86	47	70	40	2784	537
16H-6, 75	142.75	157.54	98	50	95	62	3502	522
16H-6, 80	142.80	157.59	86	33	63	45	3068	517
16H-6, 85	142.85	157.64	82	46	69	50	3142	563
16H-6, 90	142.90	157.69	132	103	103	25	3525	607
16H-6, 95	142.95	157.74	88	102	77	38	2493	604
16H-6, 100	143.00	157.79	127	67	107	52	3427	614
16H-6, 105	143.05	157.84	89	30	73	38	3114	601
16H-6, 110	143.10	157.89	113	118	105	47	2915	583
16H-6, 115	143.15	157.94	79	66	94	55	2806	570
16H-6, 120	143.20	157.99	104	89	100	54	2729	567
16H-6, 125	143.25	158.04	98	77	90	39	2553	511
16H-6, 130	143.30	158.09	67	19	61	38	2126	462
16H-6, 135	143.35	158.14	90	35	81	57	2610	477
16H-6, 140	143.40	158.19	77	26	69	48	3131	466
16H-6, 145	143.45	158.24	75	30	65	18	2042	399
16H-7, 5	143.55	158.34	127	41	105	33	2933	356
16H-7, 10	143.60	158.39	101	35	104	50	3018	345
16H-7, 15	143.60	158.44	118	38	91	28	2578	372
16H-7, 20	143.70	158.49	117	37	99	63	3164	384
16H-7, 25	143.75	158.54	119	41	100	28	3092	404
16H-7, 30	143.80	158.59	118	38	103	23	2701	415
16H-7, 35	143.85	158.64	113	38	122	16	2867	395
16H-7, 40	143.90	158.69	112	27	101	20	2592	364
16H-7, 45	143.95	158.74	94	47	92	27	2656	344

Table T3 (continued).

Core, section, top (cm)	Depth (mbsf)	Depth (mcd)	K (cps)	Ca (cps)	Ti (cps)	Mn (cps)	Fe (cps)	Susceptibility ($\times 10^{-6}$)
16H-7, 50	144.00	158.79	128	43	105	15	2289	344
16H-7, 55	144.05	158.84	116	37	88	60	2711	347
16H-7, 60	144.10	158.89	120	43	84	24	2590	342
16H-7, 65	144.15	158.94	129	39	86	16	2550	359
16H-7, 70	144.20	158.99	97	40	88	40	2601	395
16H-7, 75	144.25	159.04	132	33	87	26	2646	412
17H-1, 5	144.05	159.68	132	50	92	51	2659	377
17H-1, 10	144.10	159.73	133	53	91	42	2812	386
17H-1, 15	144.15	159.78	134	56	97	21	2614	377
17H-1, 20	144.20	159.83	114	68	96	33	2722	436
17H-1, 25	144.25	159.88	144	56	90	49	2978	482
17H-1, 30	144.30	159.93	126	35	85	43	2621	469
17H-1, 35	144.35	159.98	158	34	102	47	3392	486
17H-1, 40	144.40	160.03	152	32	101	58	3358	516
17H-1, 45	144.45	160.08	150	36	94	62	3287	520
17H-1, 50	144.50	160.13	124	32	94	37	2809	516
17H-1, 55	144.55	160.18	136	41	95	23	3158	529
17H-1, 60	144.60	160.23	73	44	76	22	2480	569
17H-1, 65	144.65	160.28	144	49	98	18	2844	580
17H-1, 70	144.70	160.33	158	107	120	20	3060	599
17H-1, 75	144.75	160.38	139	36	97	23	3282	589
17H-1, 80	144.80	160.43	134	77	105	60	4249	549
17H-1, 85	144.85	160.48	169	90	118	67	3126	518
17H-1, 90	144.90	160.53	99	97	101	20	2764	512
17H-1, 95	144.95	160.58	150	98	131	53	3254	476
17H-1, 100	145.00	160.63	104	70	94	19	2681	464
17H-1, 105	145.05	160.68	80	321	100	31	2570	451
17H-1, 110	145.10	160.73	133	213	99	17	2502	399
17H-1, 115	145.15	160.78	120	343	86	21	2526	344
17H-1, 120	145.20	160.83	119	140	89	20	2739	310
17H-1, 125	145.25	160.88	133	105	95	16	2876	271
17H-1, 130	145.30	160.93	130	37	92	53	3435	194
17H-1, 145	145.45	161.08	113	75	82	21	2605	259
17H-2, 5	145.55	161.18	130	68	91	64	3372	271
17H-2, 10	145.60	161.23	128	49	93	60	3335	319
17H-2, 15	145.65	161.28	69	109	48	21	1677	349
17H-2, 20	145.70	161.33	122	76	93	48	2526	341
17H-2, 25	145.75	161.38	113	116	82	50	2593	333
17H-2, 30	145.80	161.43	129	100	81	50	2755	332
17H-2, 35	145.85	161.48	110	93	83	52	2543	346
17H-2, 40	145.90	161.53	108	102	73	53	2522	361
17H-2, 45	145.95	161.58	130	125	86	50	2858	396
17H-2, 50	146.00	161.63	122	106	83	57	2763	454
17H-2, 55	146.05	161.68	115	111	69	48	2550	478
17H-2, 60	146.10	161.73	127	68	69	49	2837	499
17H-2, 65	146.15	161.78	140	51	96	64	3448	523
17H-2, 70	146.20	161.83	133	49	92	60	3316	506
17H-2, 75	146.25	161.88	133	40	105	66	3461	471
17H-2, 80	146.30	161.93	139	35	91	66	3287	455
17H-2, 85	146.35	161.98	139	38	94	60	3438	470
17H-2, 90	146.40	162.03	141	50	104	65	3366	486
17H-2, 95	146.45	162.08	135	63	89	61	3441	467
17H-2, 100	146.50	162.13	137	36	83	58	3165	427
17H-2, 105	146.55	162.18	134	37	87	57	3270	414
17H-2, 110	146.60	162.23	132	41	81	52	2850	388
17H-2, 115	146.65	162.28	131	46	87	58	2981	358
17H-2, 120	146.70	162.33	132	35	94	60	3153	332
17H-2, 125	146.75	162.38	116	35	91	48	2981	299
17H-2, 130	146.80	162.43	123	37	91	57	2925	297
17H-2, 135	146.85	162.48	120	38	89	51	2704	327
17H-2, 140	146.90	162.53	120	35	86	55	2877	355
17H-2, 145	146.95	162.58	124	26	95	56	3182	

CHAPTER NOTE*

N1. Dupont, L.M., Donner, B., Schneider, R., and Wefer R., submitted. Mid-Pleistocene environmental change in tropical Africa began as early as 1.05 Ma. *Geology.*

30 January 2002: Dupont, L.M., Donner, B., Schneider, R., and Wefer R., 2001. Mid-Pleistocene environmental change in tropical Africa began as early as 1.05 Ma. *Geology, 29*:195–198.

*Dates reflect file corrections or revisions.